SAPHARI

SAFE AND AUTONOMOUS PHYSICAL HUMAN-AWARE ROBOT INTERACTION

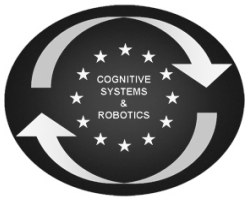

Project funded by the European Community's 7th Framework Programme (FP7-ICT-2011-7)

Grant Agreement ICT–287513

Deliverable D3.2.2 - Experimental validation of control laws for multi-dof VIA manipulators

Deliverable due date: 31 October 2015	**Actual submission date: 1 December 2015**
Start date of project: 1 November 2011	**Duration: 48 months**
Lead beneficiary for this deliverable: UNIPI	**Revision: Final**

Nature: O	**Dissemination Level: PU**
R = Report	PU = Public
P = Prototype	PP = Restricted to other programme participants (including the Commission Services)
D = Demonstrator	RE = Restricted to a group specified by the consortium (including the Commission Services)
O = Other	CO = Confidential, only for members of the consortium (including the Commission Services)

www.saphari.eu

Table of contents

1 Introduction **3**

2 Variable Stiffness Control for Oscillation Damping **5**
2.1 Problem Statement 5
2.2 One DoF VSA: Optimal Control 6
2.2.1 Concordant Terminal Conditions 8
2.2.2 Discordant Terminal Conditions 9
2.2.3 Null Terminal Position/Speed Case 9
2.3 Control of a multi DoF VSA Robot 11
2.4 Simulations and Experiments 12
2.4.1 Simulation results 13
2.4.2 Experimental Setup and Implementation 14
2.4.3 Discussion 17
2.5 Conclusions 19

3 Minimizing Energy Consumption in Soft Robots **20**
3.1 Problem Statement 20
3.1.1 Fully Actuated and Underactuated Mechanical Systems . . 21
3.1.2 Performance Indices 22
3.1.3 Optimization Problem 22
3.2 Optimization of Stiffness and Pre-Load Parameters 23
3.3 Trajectory optimization problem 27
3.4 Examples of Stiffness and Pre-load optimization 30
3.4.1 Single Joint System 30
3.4.2 Two-Link Manipulator 32
3.5 Examples of Simultaneous Optimization of Stiffness and Link Trajectories 34
3.5.1 Single Joint System 35
3.5.2 Two-Link Manipulator 36
3.6 Experimental Results 37
3.6.1 Model–Free Application: One-DoF hopping robot prototype 38
3.6.2 Two-Link Manipulator 40
3.6.3 System Description 40
3.6.4 Test Protocol and Procedure 41
3.6.5 Stiffness optimization of a Two-DoF manipulator with predefined trajectory 43
3.6.6 Simultaneous optimization of joint trajectories and stiffness of a Two-link manipulator with SEAs 46
3.7 Conclusions 48

4 Anticipaotory Control for Soft Robots **51**
4.1 Soft Robots & Anticipatory Behavior 51
4.2 Control Architecture 53

4.3 Decentralized Approach 54
4.4 Linearization 54
4.5 Stability Analysis 55
4.6 ILC Convergence Analysis 55
4.7 Experimental Results 56
4.7.1 Experiment 1 57
4.7.2 Experiment 2 58
4.7.3 Experiment 3 60
4.7.4 Experiment 4 60
4.8 Conclusions and Future Works 62

1 Introduction

The capabilities that a biologic system can show, such as running, jumping, manipulating and interacting with the surrounding world, hitting, etcetera are very far beyond what a robot can do. To reduce this gap it is essential that some features of the state-of-the-art robots are substantially improved: i) the level of robustness (both at intelligence and structural level), ii) the energy efficiency, iii) the flexibility to cope with unstructured environment, and iv) the peak performances, e.g. in terms of speed and torque.

Two of the factors that substantially contribute to the improvement of these characteristics are: control algorithms (from the lowest level to artificial intelligence) and actuation system.

In the last three decades robotic actuators gained a richer behavior. However actively impedance controlled robots (technologically available today) have clear advantages w.r.t. position servo-actuators, still they presents substantial limitations: low structural robustness against unpredictable impacts and high bandwidth required to the control system, to cite the most critical ones.The intrinsic dynamic of existing actuators have been enriched to overcome such limitations via the introduction of additional components. In Series Elastic Actuation (presented in [1]) an elastic element (with constant stiffness) was interposed between the motor and the link, while in Variable Stiffness (for a complete review see [2]) and Variable Damping (see [3]) actuators the actuation unit can physically change its dynamical parameters, i.e. stiffness and damping. This new actuation paradigm, called Soft Robotics.

Today the Series Elastic concept is available for research laboratories. An example is Baxter (see Fig. 1) a humanoid torso realized by Rethink Robotics equipped with two 7-DoF series elastic arms.

The most recent ideas like Variable Impedance are becoming available for researchers. Among them, the qb move (a modular variable stiffness servo actuator) is intended to be used as a rapid prototyping platform for experimental tests, and it allows to drastically reduce the required resources to get access to soft robotics technology. From the control point of view, the availability of Soft Robots has opened the new challenge to find suitable control policies able to exploit the full potential of this new technology.

Optimal control has been used to tackle this problem, in the safe brachistochrone task [4] or in the max speed case [5, 6]. In [7] a framework for simultaneous optimization of torque and stiffness, incorporating state and control constraints is proposed. Conventional feedback control techniques have been applied to soft robots [8] even though feedback control may substantially change the dynamic behavior of the system. An alternative approach is to take inspiration from what humans do. This idea has been pursued through two different ways: (i) tele-

Figure 1: Baxter: the adaptive, collaborative manufacturing robot realised by RethinkRobotics

impedance, which introduces the human in the control loop [9]; (ii) model free control laws [10]. The application of some of the aforementioned control tecniques to the VIAs in novel tasks has been explored, together with novel control algorithms. Experimental validations of the achieved results are reported in this work.

As pointed out in the WP8 Progress Report, it has to be noticed that the validated results, reported in this work, may be useful in a future application of VSA in the use cases investigated in the project:

- Hospital Scenario: environment with uncertainties due to both measurements and variance in the dynamical parameters of the objects with which the interaction has to be performed, high level of safety request
- Airbus and KUKA Scenarios: management of interaction with object with not regular contact surface, energy efficiency in repetitive tasks

2 Variable Stiffness Control for Oscillation Damping

In [] a model–free approach for damping control of Variable Stiffness Actuators is proposed. The idea is to take advantage of the possibility to change the stiffness of the actuators in controlling the damping. The problem of minimizing the terminal energy for a one degree of freedom spring-mass model with controlled stiffness is first considered. The optimal bang–bang control law uses a maximum stiffness when the link gets away from the desired position, i.e. the link velocity is decreasing, and a minimum one when the link is going towards it, i.e. the link velocity is increasing. Based on Lyapunov stability theorems the obtained law has been proved to be stable for a multi–DoF system. Finally, the proposed control law has been tested and validated through experimental tests.

2.1 Problem Statement

The dynamic equation of a manipulator with elastic joints is:

$$\begin{aligned} M(q)\ddot{q} + C(q,\dot{q})\dot{q} + G(q) &= f(q-\theta,\sigma) - B\dot{q} \\ I\ddot{\theta} + D\dot{\theta} &= -f(q-\theta,\sigma) + u \end{aligned} \tag{1}$$

where $q \in \mathbb{R}^n$ is the link configuration vector and $\theta \in \mathbb{R}^m$ the motor configuration vector. $M(q) \in \mathbb{R}^{nxn}$ is the inertia matrix of the manipulator, $C(q,\dot{q}) \in \mathbb{R}^{nxn}$ is the centrifugal/Coriolis matrix, $G(q) \in \mathbb{R}^n$ the gravity effect and $B \in \mathbb{R}^{nxn}$ the matrix of the viscous friction in the joints. $I \in \mathbb{R}^{mxm}$ and $D \in \mathbb{R}^{nxn}$ are respectively the actuation inertia and the damping matrix. Finally, u is the control input. With $f(q-\theta,\sigma)$ we model the action of the elastic elements that realise the coupling between the motors and the links. In this setting σ represents an input for stiffness control. For several VSAs it holds:

$$f(q-\theta,\gamma) = -K(\gamma)(q-\theta), \tag{2}$$

where $K(\gamma) = \mathrm{diag}(k(\gamma))$ is the stiffness matrix of the elastic transmissions. For example, in an antagonistic VSA, the model (2) is valid around an equilibrium

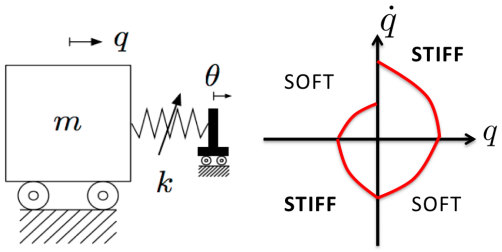

Figure 2: Left: schematic of a 1 DoF soft actuator used for the optimal control problem. Right: Optimal stiffness switching control provided in this work.

position, with $\gamma = \frac{\theta_{m,1}-\theta_{m,2}}{2}$ and $\theta = \frac{\theta_{m,1}+\theta_{m,2}}{2}$, where $\theta_{m,1}$ and $\theta_{m,2}$ are the position vectors of the two prime movers of each VSA of the robot. In the following we assume that $f(q-\theta,\gamma)$ has the form given in (2) and that $k(\gamma)$ is the vector control input.

The problem we address in this paper is to find a model-free policy for adjusting the stiffness $k(\gamma)$ for damping control of a variable stiffness robot, the model thereof can be described by the (1).

2.2 One DoF VSA: Optimal Control

From (1), the typical dynamic equation for a single DoF VSA actuator is:

$$\ddot{q} + w^2 (q - \theta) = 0\,, \tag{3}$$

where q is the link position, θ is the motor position, $w = \sqrt{k/m}$ is the natural frequency of the system, m is the link inertia, and k is the stiffness. It is worth noting that a damping parameter is not considered in (3). On the left of Fig. 2 a representation of the model in exam is reported.

Given a final time T, in the following we consider $\theta = \hat{q},\ \forall t \in [0, T]$, where $\hat{q}$ represents the desired link terminal position.

Given the state vector $x(t) = [x_1,\ x_2]^T = [q-\theta,\ \dot{q}]^T \in \mathbb{R}^2$, the control input $u(t) = k \in U = [k_{min}, k_{max}]$ with k_{min} and k_{max} minimum and maximum stiffness achievable by the VSA respectively. The system dynamics in state form is:

$$\dot{x} = f(x,u) = \begin{bmatrix} x_2(t) \\ -w^2 x_1(t) \end{bmatrix}. \tag{4}$$

Having damping effect means to decrease the mechanical energy of the system. This can be efficently obtained by minimizing the following quadratic cost function:

$$\phi(x(T)) = \frac{x_1^2(T)}{2} + \frac{x_2^2(T)}{2}\,,$$

for a fixed terminal time T.

Finally, the optimal control problem is:

$$\begin{array}{l} \min_{u(t)} \phi(x(T)) \\ \dot{x}(t) = f(x,u) \\ x(0) = x_0 \\ 0 \le k_{min} \le u(t) \le k_{max} \end{array},$$

where $x_0 = [x_{0,1}\, x_{0,2}]^T$ is the vector of the initial conditions.

The associated Hamiltonian function [11] is then:

$$H = \lambda^T f(x,u) = \lambda_1(t) x_2(t) - u(t)/m \lambda_2(t) x_1(t)\,, \tag{5}$$

where $\lambda = [\lambda_1,\ \lambda_2]^T \in \mathbb{R}^2$ is the costate vector.

According to the Pontryagin Maximum Principle (PMP) in [11], necessary conditions on the optimal control $u(t)$ can be derived by minimising (5). Since the Hamiltonian is linear on $u(t)$ we can conclude that the optimal control is bang–bang like according to the following law:

$$u(t) = \begin{cases} k_{max} & \text{when} \quad \lambda_2(t)x_1(t) > 0, \\ k_{min} & \text{when} \quad \lambda_2(t)x_1(t) < 0. \end{cases} \tag{6}$$

Hence, the switching function of the Hamiltonian is $\sigma(t) = x_1(t)\lambda_2(t)$ and a switching instant $t_s \in [0,\ T]$ is such that $\sigma(t_s) = 0$.

From the PMP optimality conditions the costate dynamics and terminal conditions are:

$$\dot{\lambda}(t)^T = -\frac{\partial H(x(t),u(t))}{\partial x(t)} = \begin{bmatrix} w^2\lambda_2(t) \\ -\lambda_1(t) \end{bmatrix} \tag{7a}$$

$$\lambda(T) = \frac{\partial \phi(x(T))}{\partial x(T)} = \begin{bmatrix} x_1(T) \\ x_2(T) \end{bmatrix}. \tag{7b}$$

Since the stiffness (hence w) is piecewise constant, see (6), the states and costates dynamics can be integrated in any time interval of amplitude Δt between two stiffness consecutive switches, i.e. *switching interval*. Hence, from (4) and (7a) for $t \in (0, \Delta t)$ we obtain:

$$x_1(t) = \bar{x}_1 \cos[w(t-\Delta t)] + \frac{\bar{x}_2}{w}\sin[w(t-\Delta t)], \tag{8a}$$

$$x_2(t) = \bar{x}_2 \cos[w(t-\Delta t)] - \bar{x}_1 w \sin[w(t-\Delta t)], \tag{8b}$$

$$\lambda_1(t) = \bar{\lambda}_1 \cos[w(t-\Delta t)] + \bar{\lambda}_2 w \sin[w(t-\Delta t)], \tag{8c}$$

$$\lambda_2(t) = \bar{\lambda}_2 \cos[w(t-\Delta t)] - \frac{\bar{\lambda}_1}{w}\sin[w(t-\Delta t)], \tag{8d}$$

where $\lambda(\Delta t) = [\bar{\lambda}_1,\ \bar{\lambda}_2]^T$ and $x(\Delta t) = [\bar{x}_1,\ \bar{x}_2]^T$.

The optimal control problem can hence be solved computing the optimal switching laws, i.e. when and under which conditions the control switches from the maximum to the minimum value and vice–versa.

The amplitude Δt of a switching interval can be computed considering a generic final state $(\bar{x}_1, \bar{x}_2)$, a generic final costate $(\bar{\lambda}_1, \bar{\lambda}_2)$, the last switching instant t_s (before Δt) and one of the two switching conditions $x_1(t_s) = 0$ or $\lambda_2(t_s) = 0$. Without loss of generality we consider the origin t_s of Δ_t as $t_s = 0$. Indeed, from (8), the

amplitude of the switching interval:

$$\Delta_{tx} = \frac{2}{w_x} \arctan\left(-\frac{\bar{x}_2}{\bar{x}_1 w_x} + \sqrt{1 + \frac{\bar{x}_2^2}{\bar{x}_1^2 w_x^2}} \right) \text{ for } x_1(t_s) = 0, \tag{9}$$

$$\Delta_{t\lambda} = \frac{2}{w_\lambda} \arctan\left(\frac{\bar{\lambda}_1}{\bar{\lambda}_2 w_\lambda} + \sqrt{1 + \frac{\bar{\lambda}_1^2}{\bar{\lambda}_2^2 w_\lambda^2}} \right) \text{ for } \lambda_2(t_s) = 0. \tag{10}$$

An equivalent but less informative form is:

$$\Delta_{tx} = \frac{1}{w_x} \arctan\left(\frac{\bar{x}_1 w_x}{\bar{x}_2} \right), \tag{11}$$

$$\Delta_{t\lambda} = \frac{1}{w_\lambda} \arctan\left(-\frac{\bar{\lambda}_2 w_\lambda}{\bar{\lambda}_1} \right), \tag{12}$$

where w_x is the pulsation of the system in a Δ_{tx}, and w_λ in a $\Delta_{t\lambda}$ respectively.

By applying condition (7b) in equations (11) and (12), one of the two amplitude is negative based on the sign of the switching function in T. Thus, the sign of the final state $x(T)$ influences the condition of the last switch of the sequence before T:

$$\text{if } x_1(T)x_2(T) > 0, \text{ it holds } x_1(t_s) = 0, \tag{13}$$

$$\text{if } x_1(T)x_2(T) < 0, \text{ it holds } \lambda_2(t_s) = 0. \tag{14}$$

The influence of final state on the last switching condition will be applied for any switching interval Δt to reconstruct all the switches occurrences.

2.2.1 Concordant Terminal Conditions

Suppose that after n switches the terminal state verifies $x_1(T)x_2(T) > 0$. From (8) and (13) the state and costate values at the last switching instant, denoted by t_{s_n}, are:

$$\begin{array}{ll} x_{1_n} = 0 & x_{2_n} = \sqrt{x_{2T}^2 + x_{1T}^2 w_x^2} \\ \lambda_{1_n} = \frac{x_{2T} x_{1T}(1 - w_x^2)}{\sqrt{x_{2T}^2 + x_{1T}^2 w_x^2}} & \lambda_{2_n} = \frac{x_{2T}^2 + x_{1T}^2}{\sqrt{x_{2T}^2 + x_{1T}^2 w_x^2}}, \end{array} \tag{15}$$

where $x(t_{s_n}) = [x_{1_n}, x_{2_n}]^T$, $\lambda(t_{s_n}) = [\lambda_{1_n}, \lambda_{2_n}]^T$ and w_x is the pulsation in the switching interval $[t_{s_n}, T]$, i.e., there are no other switches between t_s and T. It follows that a generic instant of time t_i, $t_s < t_i < T$, in which $x_1(t_i) = 0$ or $\lambda_2(t_i) = 0$ cannot exist. Moreover, from (13) and (15), $x_1(t_i)$ and $\lambda_2(t_i)$ can only be positive and hence, from (6), $w_x = \sqrt{\frac{k_{max}}{m}}$ that corresponds to the maximum control input. Thus, the n-th switching variables in (15) are hence univocally determined. It is worth noting that the obtained variables are the final state and costate values of the $n-1$-th switching intervals.

We analize the switching condition at the beginning of the $n-1$–th switch interval $[t_{s_{n-1}}, t_{s_n}]$.

Consider first the case in which at time $t_{s_{n-1}}$ the switch is caused by $\lambda_2(t_{s_{n-1}}) = 0$. From (10) and (15) we have

$$\Delta_{t\lambda} = \frac{2}{w_\lambda} \arctan(\alpha + \sqrt{1+\alpha^2}). \tag{16}$$

where $\alpha = \frac{x_{2T} x_{1T}(1-w_x^2)}{(x_{1T}^2 + x_{2T}^2) w_\lambda}$ and $w_\lambda = \sqrt{\frac{k_{min}}{m}}$ is the frequency in the switching interval $[t_{s_{n-1}}, t_{s_n}]$ that corresponds to the minimum control input.

Consider now the case in which at time $t_{s_{n-1}}$ the switch is still caused by $x_1(t_{s_{n-1}}) = 0$. From (9) and (15) we have $\Delta_{tx} = \frac{\pi}{w_x}$. It can be shown that for any value of w_x $\Delta_{tx} > \Delta_{t\lambda}$. Hence, the switch in $t_{s_{n-1}}$ is caused by $\lambda_2 = 0$.

2.2.2 Discordant Terminal Conditions

The same procedure can be applied for the case $x_1(T)x_2(T) < 0$ where the last switching condition is on λ_2. Considering (8) and (14), for the intervals $[t_{s_{n-1}}, t_{s_n}]$ and $[t_{s_n}, T]$, defined equivalently as the previous case, the state and costate at t_{s_n} are:

$$\begin{aligned} x_{1_n} &= -\frac{x_{2T}^2 + x_{1T}^2}{\sqrt{x_{1T}^2 + x_{2T}^2 w_\lambda^2}}, \qquad x_{2_n} = \frac{x_{2T} x_{1T}(w_\lambda^2 - 1)}{\sqrt{x_{1T}^2 + x_{2T}^2 w_\lambda^2}}, \\ \lambda_{1_n} &= -\sqrt{x_{1T}^2 + x_{2T}^2 w_\lambda^2}, \quad \lambda_{2_n} = 0. \end{aligned} \tag{17}$$

Hence, if $x_1(t_{s_{n-1}}) = 0$, the switching interval $[t_{s_{n-1}}, t_{s_n}]$ has amplitude:

$$\Delta_{tx} = \frac{2}{w_\lambda} \arctan(-\alpha + \sqrt{1+\alpha^2}), \tag{18}$$

where $\alpha = \frac{x_{2T} x_{1T}(1-w_\lambda^2)}{(x_{1T}^2 + x_{2T}^2) w_x}$.

On the other hand, in case of $\lambda_2(t_{s_{n-1}}) = 0$, the interval for the switching on λ is $\Delta_{t\lambda} = \frac{\pi}{w_\lambda}$. It can be shown that for any value of w_λ $\Delta_{t\lambda} > \Delta_{tx}$. Hence, the switch in $t_{s_{n-1}}$ is caused by $x_1 = 0$.

To conclude, the optimal switching sequence is characterized by alternate switching conditions on λ_2 and x_1. Hence, the initial conditions can be determined as a function of the final states for any number of switches n. For space limitations those computations are not herein reported. However, a similar procedure is applied next to a particular case that will be proved to play a crucial role in the definition of a model–free control law.

2.2.3 Null Terminal Position/Speed Case

We now consider the particular case of minimizing the energy at a given final time T with the additional condition that the desired amount of energy is concentrated

in the kinematic or in the elastic potential term, i.e. one of the terminal states value $x(T)$ is zero.

We start considering a generic switching interval $\delta_1 = [0, \Delta t_1]$ with $x_1(\Delta t_1) = \lambda_1(\Delta t_1) = 0$. Notice that at time Δt_1 the switching condition (13) is verified. For the alternate sequence of switching conditions we have $\lambda_2(0) = 0$, i.e. the switching condition (14) must be verified at the initial instant of δ_1. Hence, from (8d), we obtain $\Delta_t = \frac{\pi}{2w_\lambda}$ or $\lambda_2(\Delta_t) = 0$ where the latter contradicts the alternance of switches.

Moreover, for $\Delta_t = \frac{\pi}{2w_\lambda}$, from (8) the initial state and costate values are:

$$x_1(0) = -\frac{x_2(\Delta_t)}{w_\lambda}, \qquad x_2(0) = 0, \tag{19}$$

$$\lambda_1(0) = -\lambda_2(\Delta_t) w_\lambda, \qquad \lambda_2(0) = 0. \tag{20}$$

For the second case of null final speed, we consider again a generic switching interval $\delta_2 = [0, \Delta t_2]$ with $x_2(\Delta t_2) = \lambda_2(t) = 0$. At time Δt_1 the switching condition (14) is verified and hence the switching condition (14) must be verified at the initial instant of δ_2, i.e. $x_1(0) = 0$. From (8a), we obtain $\Delta t = \frac{\pi}{2w_x}$ or $x_1(\Delta t) = 0$ where the last condition contradicts the alternance of switches. Hence, from (8) the initial state and costate values are:

$$x_1(0) = 0, \qquad x_2(0) = x_1(\Delta t_2) w_x, \tag{21}$$

$$\lambda_1(0) = 0, \qquad \lambda_2(0) = \frac{\lambda_1(\Delta t_2)}{w_x}. \tag{22}$$

It is worth noting that the obtained initial conditions for δ_1 (δ_2) coincide with the assumption on the final condition of δ_2 (δ_1). We can then consider an arbitrary number n of sequences of alternate switching intervals δ_1 and δ_2 depending on the state values at time T. Indeed, in case of null final speed or position, the terminal time T coincides with the last switching time t_{s_n}. Moreover, in case of $x_1(T) = 0$ we have $[t_{s_{n-1}}, T] = \delta_1$ while if $x_2(T) = 0$ we have $[t_{s_{n-1}}, T] = \delta_2$.

The state and costate values at a generic switching time t_{s_k} can thus be obtained. For the case of null final position and for odd k we have:

$$\left(x_1\left(t_{s_k}\right), x_2\left(t_{s_k}\right)\right) = \left(-x_{2T} \frac{w_x^{(k-1)/2}}{w_\lambda^{(k+1)/2}} \sin\left(\frac{k\pi}{2}\right), 0\right),$$

$$\left(\lambda_1\left(t_{s_k}\right), \lambda_2\left(t_{s_k}\right)\right) = \left(-x_{2T} \frac{w_\lambda^{(k+1)/2}}{w_x^{(k-1)/2}} \sin\left(\frac{k\pi}{2}\right), 0\right),$$

while for even k:

$$(x_1(t_{s_k}), x_2(t_{s_k})) = \left(0, x_{2T}\frac{w_x^{k/2}}{w_\lambda^{k/2}}\cos\left(\frac{k\pi}{2}\right)\right),$$
$$(\lambda_1(t_{s_k}), \lambda_2(t_{s_k})) = \left(0, x_{2T}\frac{w_\lambda^{k/2}}{w_x^{k/2}}\cos\left(\frac{k\pi}{2}\right)\right).$$

Given the sequence of n switching intervals, in the $n-k$-th interval the switching function is $\sigma_k = x_1(t)x_2(t)p(k)$ where $p(k) = (w_\lambda/w_x)^k$ for even k and $p(k) = (w_\lambda/w_x)^{k+1}$ for odd k.

For the complementary case of null final speed, for odd k we have:

$$(x_1(t_{s_k}), x_2(t_{s_k})) = \left(0, x_{1T}\frac{w_x^{(k+1)/2}}{w_\lambda^{(k-1)/2}}\sin\left(\frac{k\pi}{2}\right)\right),$$
$$(\lambda_1(t_{s_k}), \lambda_2(t_{s_k})) = \left(0, x_{1T}\frac{w_\lambda^{(k-1)/2}}{w_x^{(k+1)/2}}\sin\left(\frac{k\pi}{2}\right)\right),$$

while for even k:

$$(x_1(t_{s_k}), x_2(t_{s_k})) = \left(x_{1T}\frac{w_x^{k/2}}{w_\lambda^{k/2}}\cos\left(\frac{k\pi}{2}\right), 0\right),$$
$$(\lambda_1(t_{s_k}), \lambda_2(t_{s_k})) = \left(x_{1T}\frac{w_\lambda^{k/2}}{w_x^{k/2}}\cos\left(\frac{k\pi}{2}\right), 0\right).$$

Given the sequence of n switching intervals, in the $n-k$-th interval the switching function is $\sigma_k = x_1(t)x_2(t)r(k)$ where $r(0) = p(0)$ and $r(k) = p(k)/w_x^2$ otherwise. Since $r(k) > 0$ the optimal stiffness control policy can be described by

$$u = \begin{cases} k_{max} \text{ if } (q-\theta)\dot{q} > 0, \\ k_{min} \text{ if } (q-\theta)\dot{q} < 0. \end{cases} \tag{23}$$

Remark 1 *In case of final null position or velocity, the switching function σ, whose sign determines the optimal switching law, does not depend on the model parameters. Hence, the obtained control law is model–free. On the right of Fig. 2 a scheme of the control law is showed. Moreover, for the considered model the control law in* (23) *can be written as $u = k_{max}$ if $\ddot{q}\dot{q} < 0$ and $u = k_{min}$ if $\ddot{q}\dot{q} > 0$ that is the opposite of the control law found [12] and [6] where the objective was to maximize the link terminal speed.*

2.3 Control of a multi DoF VSA Robot

In this section we apply the model-free stiffness control policy derived in the previous section to the VSA multi DoF robot model described by the equation (1). It

is worth to note that in (1) the damping effect is considered with the contribution $-B\dot{q}$. We assume that the motor provides a torque input u such that the motor position θ is set to bring the robot at the desired equilibrium position $\hat{q}$. In absence of gravity it is $\theta = \hat{q}$. In [13] it is shown that also in presence of gravity a $\theta \neq \hat{q}$ can be found so that q converges to $\hat{q}$. Hence, gravity does not affect the applicability of the proposed controller since it acts only on the stiffness input $k(\sigma)$, and hence from now on in the analysis we consider $\theta = \hat{q} = 0$.

In the following we motivate the application of the proposed algorithm through Lyapunov like arguments.

Consider now the state vector $x = [q, \dot{q}]^T$, the kinetic energy T, the gravitational energy U_g, and the minimum elastic energy $U_{k_{min}} = 1/2(\theta - q)^T K_{min}(\theta - q)$ of the link dynamics described by the first equation of (1) where $K_{min} = diag(k_{min})$. The following Lyapunov candidate can be derived:

$$V(x) = T + U_g + U_{k_{min}} = \frac{1}{2}\dot{q}^T M(q)\dot{q} + U_g(q) + U_{k_{min}}(\theta, q).$$

The time variation of the previous equation is:

$$\begin{aligned}\dot{V}(x) = \frac{\partial V}{\partial x}\dot{x} = \dot{q}^T M(q)\ddot{q} + \frac{1}{2}\dot{q}^T \dot{M}(q)\dot{q} + G(q)^T \dot{q} + \\ (q - \theta)^T K_{min}(\dot{q} - \dot{\theta}).\end{aligned} \tag{24}$$

By substituting (1) in (24) and considering that $\dot{M}(q) = 2C(q, \dot{q})\dot{q}$ it follows:

$$\dot{V}(x) = -\dot{q}^T B\dot{q} - \dot{q}^T (K(\gamma) - K_{min})(q - \theta). \tag{25}$$

By applying the optimal control policy given in (23) for each component of the control vector $K(\gamma)$, the (25) is negative semi-definite. Nevertheless, since the only trajectory that lays in $R = \{x | \dot{V}(x) = 0\}$ is zero is the equilibrium, by applying the Krasovskii-Lasalle theorem it is possible to conclude for the asymptotic stability of the origin.

The effect of the control law (23) in the multiple DoF system is to increase the rate of convergence to the equilibrium point since it minimises the (25), i.e. it dissipates as much energy as possible by adjusting the stiffness. It is worth noting that, even though the control law in (23) has been obtained based on the damping–free system (3), in this section it has been shown that it is stabilizing also for systems with viscosities.

2.4 Simulations and Experiments

In this section the simulation for a single DoF robot and the experiments on single and multi DoF VSA are proposed. In Fig. 3 the schemes of the considered system are reported.

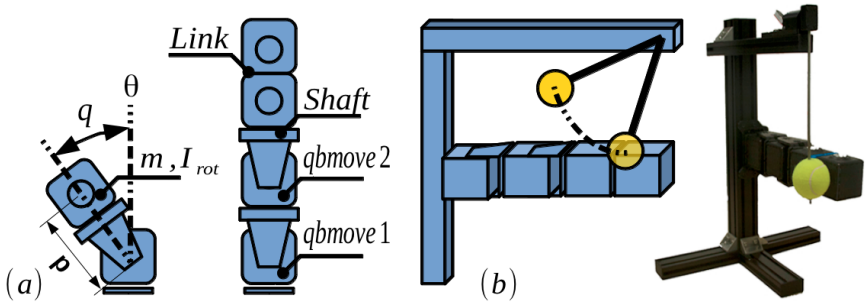

Figure 3: (a) Scheme of the 1 DoF and 2 DoF planar arms used for the simulations and experiments. The revolute joints are indicated as *qbmove* 1 and *qbmove* 2. (b) Experimental setup for the 2 DoF case.

2.4.1 Simulation results

A link of mass m with the center of mass posed at distance d is connected to a VSA which can instantaneously change the stiffness between the motor and the link in the interval $[k_{min}, k_{max}]$. A viscous friction b acts on the joint. Let θ be the position of the motor, $\hat{q}$ the equilibrium position of the link and q the link position. The actuator dynamic is neglected and gravity doesn't affect the system.

In the simulation the motor position θ is set equal to the desired link equilibrium position $\hat{q}$. A representation of the model can be observed in the 1 DoF case of in Fig. 3 (a) which is an equivalent implementation of the system presented in Fig. 2. The dynamic parameters of the system are: the mass $m = 0.226\,[K_g]$, the distance of the mass from the center of rotation $d = 0.1\,[m]$, the rotational inertia of the link $I_{rot} = 0.001[K_g m^2]$, the maximal and minimal stiffness $[K_{max}, K_{min}] = [1, 0.3]\,[Nm/\,rad]$ respectively and the module of the viscous friction $b = 0.01\,\left[Nms^2/\,rad^2\right]$. The link starts from the equilibrium configuration and receives an impulsive external torque of $1\,Nm$ after $0.2\,s$. In the first and second simulations the actuator is controlled to generate a constant stiffness, at minimum and maximum values respectively. Finally, in the third simulation the stiffness is regulated according to the control law (23). In Fig. 4 the results of the simulations are shown for the three different inputs. The time, from the impact instant, to reach an error position that remains in a neighbourhood of the origin of radius $0.05\,rad$, has been evaluated. Such settling times are indicated in figure with vertical dot lines and their values are: $2.06\,s$ for the minimum stiffness case, $2.18\,s$ for the maximum stiffness case, and $0.93\,s$ for the optimal control case (where the impact was at $t = 0.2s$). In this case, the stiffness switching control produces an improvement of 100% of the settling time with respect to the constant stiffness cases.

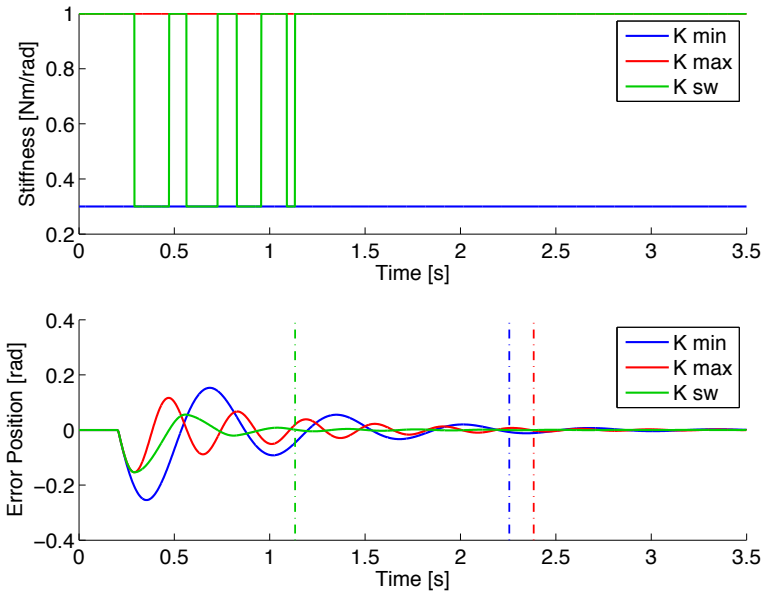

Figure 4: Top: stiffness evolution under constant minimum and maximum inputs and under the proposed control law. Bottom: evolutions of the link error positions.

2.4.2 Experimental Setup and Implementation

Two planar robotics arms, 1 DoF and 2 DoF respectively, have been realised with qbmove actuators based on the VSA Cube [14] (see [15] for the datasheet with the main actuators characteristics). The first arm uses another qbmove actuator connected to the first by a shaft as inertia. The second arm uses two qbmove actuators connected to the last active joint by a shaft as inertia. The systems are mounted on a structure to be not influenced by the gravity as shown in Fig. 3. On the top of the structure a pendulum is used to simulate the disturbance, i.e. an impact at the end of the arm.

For the one degree of freedom experiment we compared four different cases: uncontrolled oscillation of the system, PID control based on error position of the link for a constant stiffness reference (half of the range of the qbmove), the bang-bang position control presented in [13] with the bring back motion generated by a PID, and the control law obtained with the proposed approach. This has been repeated for two different inertia values. The stiffness control is realised by adjusting the stiffness preset $\gamma = (\theta_{m,1} - \theta_{m,2})/2$. This is possible since the control is bang–bang like and the stiffness of the qbmove is a monotonic function of the preset. In Fig. 5 we present a comparison of the link position evolution of the 1 DoF system (with 1-actuator-link) in case of an impact after 1 second under different controls: system at maximum stiffness with null control, PID control, the bang–bang position

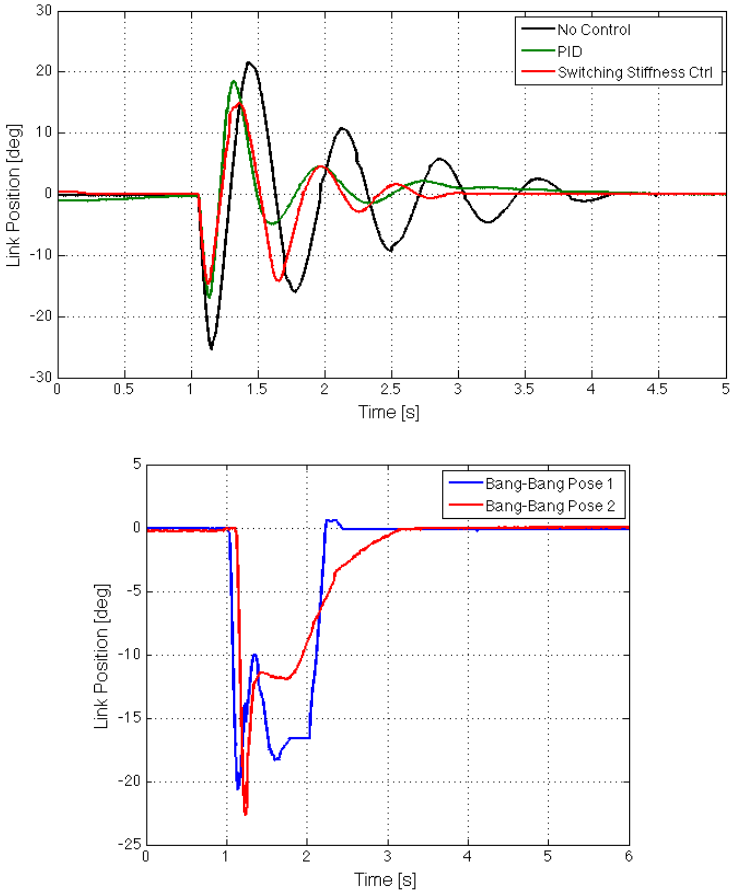

Figure 5: Top: Link position evolution for different control strategies applied to the 1 DoF system. In red, the evolution in case of the control law proposed in this paper. Bottom: Link position evolution for two different implementation of Bang–Bang position control.

control presented in [13] and the proposed stiffness switching control law. The PID control and the one used for the bring back phase in the bang–bang position control, in [13], have been experimentally tuned. The tuned PID shows the best result in term of settling time which is comparable to the stiffness switching control. In the bottom of Fig. 5 two implementation of the Bang–Bang position control are shown. Those controls differ in the timing of the bring back phase and PID. The performance of the control is influenced by the dynamic of the actuator and the control used in the bring back motion.

In Fig. 6 a further comparison is implemented where the inertia of the link is doubled. The proposed control law is now compared with two other PID controls: the PID1 tuned on the new system characteristics and PID2 is the same PID control law used in the previous set of experiments with lower inertia. The stiffness

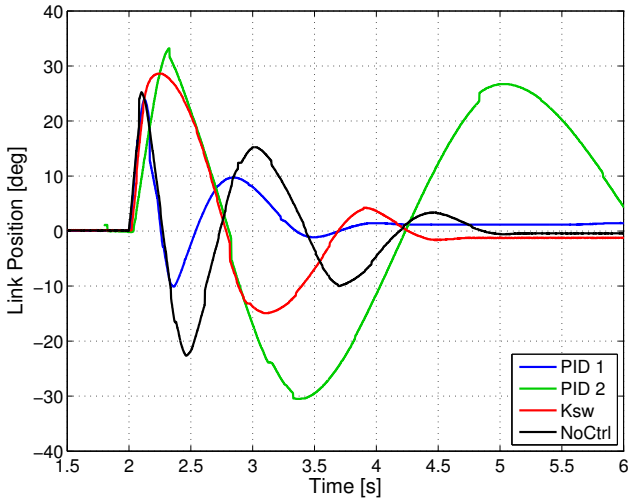

Figure 6: Link position evolution for different control strategies applied to the 1 DoF system in case of a (almost) double link inertia w.r.t. the case presented in Fig. 5. The PID control presents the best performance but it is tuned on the particular system. The stiffness switching control K_{sw} presents a performance comparable to the performance of PID 1 despite the increased inertia.

switching control K_{sw} shows robustness to the inertia variation and a performance comparable with the PID1 opportunely tuned. On the other hande, the PID2 shows instability.

Since the qbmove has a stiffness variation time of 0.1 seconds from the minimum to the maximum stiffness values, when the link oscillations happen at a too high frequency the stiffness cannot change instantaneously. For this reason it has been implemented a stiffness control law based on thresholds (experimentally evaluated) on the position and the velocity of the link in order to anticipate the stiffness switchings. A comparison between the theoretical and the threshold–based approach for the one degree of freedom case is reported in Fig. 7. In Fig. 8 and 9 we present the experimental results for the two degrees of freedom case and the comparison between the controlled system (with the law (23)) and the uncontrolled system with low and high stiffness configurations. The comparison shows that the switching control law guarantees an improvement of 25% of the settling time w.r.t the stiff case.

It is worth noting that in Fig. 7 and 8 the stiffness is measured in $[deg]$ in the range $[0, 35]$ deg that is equivalent to a stiffness values of $[0.3, 13]\,Nm$ on the output shaft.

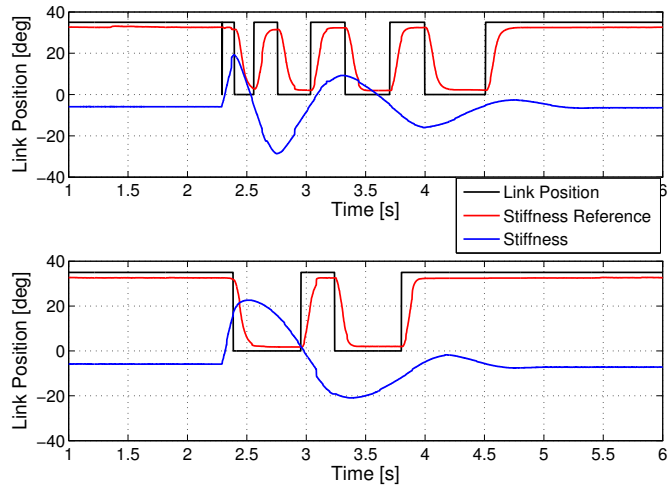

Figure 7: Link position and preset evolution for the one DoF case with the theoretical control (top) and thresholds–based control (bottom) to anticipate the switching instants

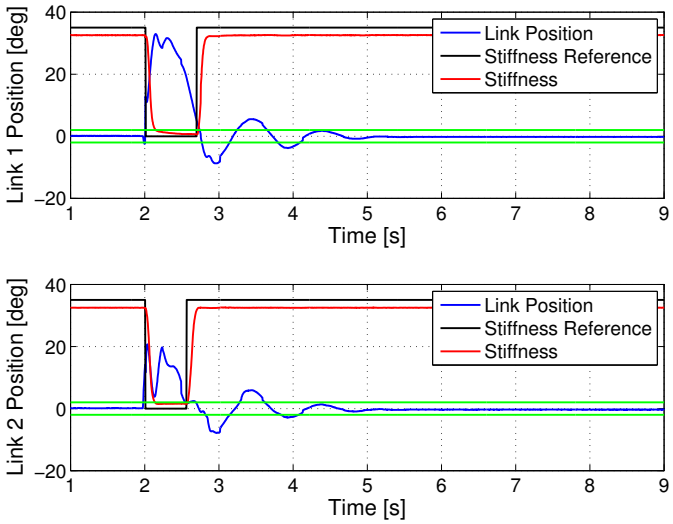

Figure 8: Links position evolution for the stiffness switching control applied to the two DoF case. The reference switchings of the preset are reported in black while the measured preset is in red. The settling time from the impact to reach the desired position with an error of ± 2deg (in green) is $T_{sw1} = 2.098s$ and $T_{sw2} = 2.078s$ for the first and second link respectively.

2.4.3 Discussion

In the following we discuss advantages and drawbacks of the proposed control approach w.r.t. existing controllers.

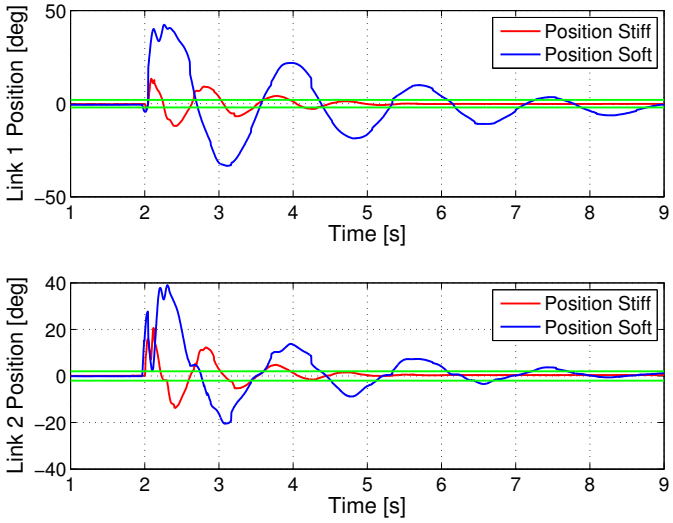

Figure 9: Links position evolution for the uncontrolled 2 DoF system with constant preset. The evolution of the links after the impact in case of maximum preset are indicated in red, while in case with minimum preset are indicated in blue. The settling times in the stiff case are $T_{stiff_1} = 2.438s, T_{stiff_2} = 2.032s$ for first and second link respectively, while for the soft case $T_{soft_1} > 8s$, $T_{soft_2} = 5.738s$.

An advantage is the fact that the stiffness control law does not depend on the model of the system, furthermore it relies on the detection of state events (i.e. zero crossing of deflection and velocity). Furthermore, even though the dynamical system differs from the nominal one the obtained control law can be still applied. While, in this case, optimality cannot be guaranteed anymore, the Lyapunov based analysis proves that using the control law in case of damping at the link side the settling time of the system is improved. Moreover the proposed approach can be profitably used to stabilise a multidof VSA robot. These characteristics, belonging also to the controller presented in [13], make it relatively easily applicable to a variety of systems since it does not requires a carefully identified model. A difference w.r.t. the law found in [13] is that the stiffness switching control law does not require a further control to bring the system to the desired position.

An important limitation is that if the stiffness regulation time is limited, the controller performance decays and the stiffness switchings must be anticipated to achieve better damping performances (see Fig. 7). Since the controller does not take into account the inertia coupling a model-based controller (provided with an accurate model) can have higher performance.

A further approach to control VSA robots that has been proposed in recent years is the tele-impedance. In this approach the stiffness regulation of the robot is teleoperated by a human being. In [9] it has been studied the task of catching a ball with

a Kuka LIghtWeight robot where the stiffness is regulated with the tele-impedance approach. The reported data (Fig. 6 Tele-Impedance and Fig.7 End Point Stiffness in section IV Results in [9] present a peak of End Point stiffness at the beginning of the task. The temporal evolution of the stiffness and error position of the end effector seems to suggest that the stiffness is increased when the end effector of the robot is getting away from the desired position and it is decreased when the end effector is coming back toward the desired position. This is similar to the behaviour of the system under the control policy presented in this paper. However, further studies are required to drawn proper conclusions.

2.5 Conclusions

In this paper a model–free approach for damping control of VSA robots through stiffness variation has been proposed. The stiffness control law has been derived by analytically solving the optimal control problem of minimizing the terminal energy for a one DoF spring-mass model with controlled stiffness. The stiffness switching control law uses a maximum stiffness when the link gets away from the desired position and a minimum one when the link is going towards it. A preliminary analysis of data presented in the literature seems to suggest that the proposed law could explain how humans change their stiffness for oscillation damping. Based on Lyapunov stability theorems the obtained law has been proved to be stable for a multi–DoF system. Simulations and experimental tests that validate the theoretical results have been reported.

3 Minimizing Energy Consumption in Soft Robots

In this work we consider the problem of reducing the energy consumption of compliant mechanical systems during desired motions, e.g. cyclic, such as those required in many robotic tasks. We start by proposing a general method that determines the optimal soft actuation parameters, i.e. stiffness value and spring pre-load, that minimize a cost functional for given link trajectories. We provide simulations and an experimental validation of the analytic results obtained, applying them to a two-link compliant manipulator platform actuated by SEAs, which performs a repetitive Pick and Place task. We then tackle the more complex problem of concurrently optimizing soft actuation parameters and link trajectories. We apply this procedure to the two-link manipulator to determine the optimal trajectories by using numerical optimization tools. At the end, we show by simulations and experiments that the simultaneous optimization of stiffness and trajectories improves the performance of the system in terms of the energy consumption with respect to the case in which only the stiffness is optimized.

3.1 Problem Statement

Mechanical systems can be fully actuated, if there are as many actuators as Degrees of Freedom (DoF) or underactuated, if there are less control inputs than DoF (see [16]). Moreover, depending on how and where the springs are placed in the system, the dynamics of a mechanical system can assume particular forms. In this section, after showing the different mechanical systems considered in this paper and their dynamical models, we will discuss the cost functionals used to quantify the energy

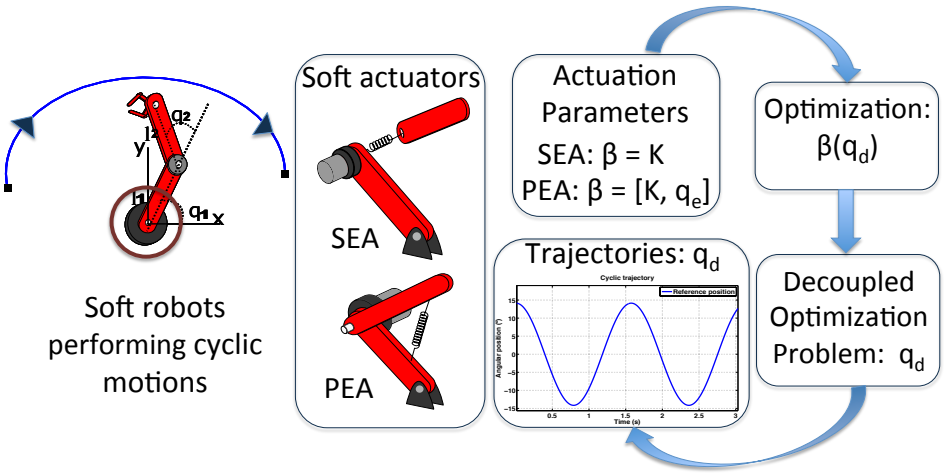

Figure 10: Robots with soft actuators. Problem decoupling: Optimization of actuation parameters and trajectory optimization problem

consumption and finally we will state the optimization problem.

3.1.1 Fully Actuated and Underactuated Mechanical Systems

- Fully Actuated Mechanical Systems: Let us consider a fully actuated compliant mechanical system actuated by PEAs. In this case, the number of DoFs is equal to the number of actuators. Indicating by $q \in \Re^n$ the generalized coordinates representing the configuration of the system and by $\tau \in \Re^n$ the generalized torque provided by actuators, the dynamics can be written as

$$f(\ddot{q},\dot{q},q,t) = K(q_e - q) + \tau\,, \tag{26}$$

  where $q_e \in \Re^n$ is the spring pre-load and $K \in \Re^{n\times n}$ is the stiffness matrix. The term $f(\ddot{q},\dot{q},q,t)$ includes inertia, coriolis, and gravity terms[1].

Consider now a mechanical system actuated by SEAs, which is underactuated. Indicating by $\theta \in \Re^n$ the motor positions and by J_m the inertia matrix of the motors, the dynamics can be written as[2]

$$f(\ddot{q},\dot{q},q,t) = -K(q-\theta) \tag{27}$$

$$J_m\ddot{\theta} = K(q-\theta) + \tau\,, \tag{28}$$

Notice that the use of SEAs instead of PEAs increases the number of DoFs, which become $2n$, while the control inputs remain n.

Remark 2 *Underactuated Mechanical Systems*
For particular mechanical systems there may be further non-actuated DoFs, e.g. the position and orientation of humanoids w.r.t. a fixed reference frame. Let $z \in \Re^m$ be those DoFs and assume the system is actuated by SEAs. The dynamics in this case can be written as

$$f_u(\ddot{z},\dot{z},z,\ddot{q},\dot{q},q,t) = 0 \tag{29}$$

$$f_a(\ddot{z},\dot{z},z,\ddot{q},\dot{q},q,t) = -K(q-\theta) \tag{30}$$

$$J_m\ddot{\theta} = K(q-\theta) + \tau, \tag{31}$$

where (29) *represents the non-actuated dynamics, whereas* (30) *and* (31) *represent the underactuated dynamics.*

Of course, if PEAs are used, the dynamics becomes

$$f_u(\ddot{z},\dot{z},z,\ddot{q},\dot{q},q,t) = 0 \tag{32}$$

$$f_a(\ddot{z},\dot{z},z,\ddot{q},\dot{q},q,t) = -K(q_e - q) + \tau\,. \tag{33}$$

[1] the actuator itself is considered rigid

[2] viscous friction term is not written to make analytical calculations simpler. Adding the corresponding term does not change the procedure. In the experimental tests presented in this paper, viscous friction is indeed considered.

By integration, in the SEA case from (29) *it is possible to find z as a function of the desired trajectories* $q_d(t)$*. Hence, by substituting in* (30) *and* (31)*, we obtain*

$$f(\ddot{q}_d, \dot{q}_d, q_d, t) = -K(q_d - \theta) \tag{34}$$

$$J_m\ddot{\theta} = K(q_d - \theta) + \tau\,, \tag{35}$$

which has the same form of (27) *and* (28)*. Similarly, in the PEA case from* (32) *we may obtain* (26)*. Therefore, the analysis proposed herein is valid for every underactuated system.*

3.1.2 Performance Indices

To quantify the performance of the mechanical systems and hence to determine the optimal joint stiffness $\hat{K}$ and pre-load $\hat{q}_e$ values (the latter for PEAs), as well as the optimal link trajectories $\hat{q}(t)$, two different cost functionals will be considered, namely, Squared Power J_1 and Squared Torque J_2.

- Squared-Power Index
  Assume that a motor is not able to recover energy from negative work, then it spends energy if the mechanical power is positive or negative. Consider that the motor requires a torque τ to generate a change of position of θ, with velocity $\dot{\theta}$. The mechanical power is $P = \tau\dot{\theta}$. The proposed index represents the squared mechanical power accumulated in a period T.

  $$J_1 = \sum_{j=1}^{n} \int_0^T (\tau_j(t)\dot{\theta}_j(t))^2 dt\,, \tag{36}$$

  Notice that in the case of PEA $\dot{\theta}_j$ changes to $\dot{q}_j$.

- Squared-Torque Index
  There is a direct relation among the torque required to produce a motion and the energy consumed by the motors when performing that motion. The proposed index represents the square of the torque τ required to move the j-th joint in a period T.

  $$J_2 = \sum_{j=1}^{n} \int_0^T \tau_j^2(t) dt\,. \tag{37}$$

The physical relevance of these indices will be discussed in the next section.

3.1.3 Optimization Problem

In this paper we consider the problem of determining optimal link stiffness $\hat{K}$ and/or pre-load $\hat{q}_e$, as well as optimal link trajectories $\hat{q}(t)$, such that the cost func-

tionals J_1 or J_2, are minimized, i.e. the following optimization problem:

$$\min_{\tau(t),\beta,q} J_i(q,\dot{q},\ddot{q},\beta(q)), \qquad i \in \{1,2\}$$
$$s.t. \begin{cases} \text{Dynamics equations} \\ q(t) = q(t+T) \\ \xi_1(q,\dot{q},\ddot{q}) \leq 0 \\ \xi_2(q,\dot{q},\ddot{q}) = 0 \\ \beta_m \leq \beta \leq \beta_M \end{cases} \tag{38}$$

where the term *Dynamics equations* corresponds to (26) or both (27) and (28), depending on the actuation case. β is a vector containing both joint stiffness K and pre-load q_e in case of PEAs, whose limits are $\beta_M = [K_M, q_{e,M}]$ and $\beta_m = [K_m, q_{e,m}]$; or only stiffness K in case of SEAs, whose limits are $\beta_M = K_M$ and $\beta_m = K_m$. Finally, the nonlinear constraints ξ_1 and ξ_2, which depend on the variables q, $\dot{q}$, and $\ddot{q}$, define the task. For instance, in the pick and place task for a two-link planar manipulator, we constrain the motion of the end-effector to the line between two specific points.

3.2 Optimization of Stiffness and Pre-Load Parameters

In this section, we derive the actuation parameters of the mechanical systems presented previously, actuated by SEAs or PEAs. In the following, we assume that $K = \text{diag}[K_1, K_2, ..., K_n]$ and $J_m = \text{diag}[J_{m1}, J_{m2}, ..., J_{mn}]$, which is valid for the majority of the mechanical systems. Once the optimal actuation parameters are obtained as a function of the chosen set of desired link trajectories $q_d(t)$, we show how the problem of optimizing the actuation parameters and the link trajectories can be cast in a simpler problem where the optimization regards only the trajectories, which can then be optimized for instance by Sequential Quadratic Programming [17], Nonlinear Programming or other suitable optimization methods [18]. At the end, a solution for the trajectory optimization problem is also provided.

For the sake of space, we only present the procedure to derive the optimal stiffness in case of mechanical systems actuated by SEAs. The same procedure presented here can be applied with slight differences to the other mechanical systems actuated by SEA or PEA and considering indices (36) or (37).

Let us assume that link trajectories $q(t) = q_d(t)$ and its first $\dot{q}(t) = \dot{q}_d(t)$ and second $\ddot{q}(t) = \ddot{q}_d(t)$ derivatives are given, and consider a mechanical system described by (27) and (28), which can be written as follows, because the matrices K and J_m are assumed to be diagonal,

$$f_j(\ddot{q}_d, \dot{q}_d, q_d, t) = -K_j(q_{d,j} - \theta_j), \tag{39}$$
$$J_{m_j}\ddot{\theta}_j = \tau_j + K_j(q_{d,j} - \theta_j), \tag{40}$$

for $j = 1, 2, \ldots, n$, which denotes the j-th actuator of the system.

Remark 3 *In this paper we find an analytical solution in cases where it is clear to gain insight, i.e. assuming that K and J_m are diagonal matrices. However, for systems whose stiffness or motor's inertia matrices are not diagonal,* (39)*, and* (40) *are not valid. For example, [19] presents a compliant underactuated finger with non-diagonal stiffness matrix. In these cases, the analysis can be carried out if the stiffness matrix is invertible.* ◇

From (39) we obtain the motor position and then its velocity and acceleration,

$$\theta_j = K_j^{-1} f_j(\ddot{q}_d, \dot{q}_d, q_d, t) + q_{d,j}\,, \tag{41}$$

$$\dot{\theta}_j = K_j^{-1} \dot{f}_j(\ddot{q}_d, \dot{q}_d, q_d, t) + \dot{q}_{d,j}\,, \tag{42}$$

$$\ddot{\theta}_j = K_j^{-1} \ddot{f}_j(\ddot{q}_d, \dot{q}_d, q_d, t) + \ddot{q}_{d,j}\,. \tag{43}$$

Replacing (41) and (43) in (40), the j-th motor torque required to track the desired trajectory $q_{d,j}(t)$ is

$$\tau_j = J_{m_j}(K_j^{-1} \ddot{f}_j(\ddot{q}_d, \dot{q}_d, q_d, t) + \ddot{q}_{d,j}) + f_j(\ddot{q}_d, \dot{q}_d, q_d, t)\,, \tag{44}$$

which corresponds to the inverse dynamics of the system.

We rewrite the cost index J_1 in terms of $q_d(t)$, its derivatives, and the stiffness K. The element related to the j-th actuator is

$$J_{1,j} = \int_0^T (\tau_j(t)\dot{\theta}_j(t))^2 dt\,. \tag{45}$$

By substituting (42) and (44) in (45), we obtain

$$\begin{aligned} J_{1,j} &= \int_0^T (\tau_j(t)\dot{\theta}_j(t))^2\, dt \\ &= \int_0^T ((J_{m_j} K_j^{-1} \ddot{f}_j + J_{m_j}\ddot{q}_{d,j} + f_j)(K_j^{-1}\dot{f}_j + \dot{q}_{d,j}))^2\, dt \\ &= \int_0^T \left(\frac{a_j(t)}{K_j^2} + \frac{b_j(t)}{K_j} + c_j(t) \right)^2 dt \end{aligned}$$

where $a_j(t) = J_{m_j}\ddot{f}_j\dot{f}_j$; $b_j(t) = J_{m_j}(\ddot{f}_j\dot{q}_{d,j} + \dot{f}_j\ddot{q}_{d,j}) + f_j\dot{f}_j$; and $c_j(t) = J_{m_j}\ddot{q}_{d,j}\dot{q}_{d,j} + f_j\dot{q}_{d,j}$.

$J_{1,j}$ depends only on the stiffness K_j of the j-th actuator, hence

$$\min_K J_1 = \sum_j \min_{K_j} J_{1,j}\,.$$

The optimal solution for each K_j is such that $\frac{\partial J_{1,j}}{\partial K_j} = 0$ which, after some algebra becomes

$$4A_{S,j} + 3K_j B_{S,j} + 2C_{S,j}K_j^2 + D_{S,j}K_j^3 = 0\,, \tag{46}$$

where

$$A_{S,j} = \int_0^T a_j^2(t)dt\,, \quad B_{S,j} = \int_0^T 2a_j(t)b_j(t)dt$$
$$C_{S,j} = \int_0^T (2a_j(t)c_j(t) + b_j^2(t))dt$$
$$D_{S,j} = \int_0^T 2b_j(t)c_j(t)dt\,.$$

$A_{S,j}$, $B_{S,j}$, $C_{S,j}$, and $D_{S,j}$ depend only on $q_{d,j}$, $\dot{q}_{d,j}$, $\ddot{q}_{d,j}$, and $f(\cdot)$ which are assumed to be known.

For the cost functional J_2, the j-th element related to the j-th actuator is

$$J_{2,j} = \int_0^T \tau_j^2(t)dt\,.$$

After substituting (44), and with some algebra, we obtain

$$J_{2,j} = \frac{F_{S,j}}{K_j^2} + \frac{G_{S,j}}{K_j} + H_{S,j}\,, \tag{47}$$

where

$$F_{S,j} = \int_0^T (J_{m_j}\dddot{f}_j)^2 dt\,,\; H_{S,j} = \int_0^T (J_{m_j}\ddot{q}_{d,j} + f_j)^2 dt\,,$$
$$G_{S,j} = \int_0^T 2J_{m_j}\dddot{f}_j(J_{m_j}\ddot{q}_{d,j} + f_j)dt\,.$$

Also in this case $J_{2,j}$ depends only on the stiffness K_j of the j-th actuator. Hence,

$$\min_K J_2 = \sum_j \min_{K_j} J_{2,j}\,.$$

The optimal solution for each K_j is such that $\frac{\partial J_{2,j}}{\partial K_j} = 0$, obtaining

$$\hat{K}_j = -2\frac{F_{S,j}}{G_{S,j}}\,. \tag{48}$$

Table 1 summarizes the expressions for the optimal actuation parameters for indices J_1 and J_2 either for SEAs and for PEAs.

The optimal value for stiffness K and pre-load q_e obtained before are not necessarily inside the admissible range of values. In this case, the optimal values will be on the boundary of the admissible set of values.

	J_1	J_2
SEA	A solution of (46)	$\hat{K}_j = -2\frac{F_{S,j}}{G_{S,j}}$
PEA	$\hat{K}_j = \frac{B_{P,j}E_{P,j} - 2C_{P,j}D_{P,j}}{4D_{P,j}F_{P,j} - E_{P,j}^2}$ $\hat{q}_{e,j} = \frac{C_{P,j}E_{P,j} - 2B_{P,j}F_{P,j}}{2C_{P,j}D_{P,j} - B_{P,j}E_{P,j}}$	$\hat{K}_j = \frac{\hat{q}_{e,j}H_{P,j} - I_{P,j}}{2(\hat{q}_{e,j}^2 T + L_{P,j} - \hat{q}_{e,j}M_{P,j})}$ $\hat{q}_{e,j} = \frac{H_{P,j} + \hat{K}_j M_{P,j}}{2\hat{K}_j T}$
	Parameters	
	$A_{P,j} = \int_0^T f_j^2 q_{d,j}^2 dt\,,$ $C_{P,j} = \int_0^T 2f_j \dot{q}_{d,j}^2 q_{d,j} dt\,,$ $E_{P,j} = \int_0^T 2\dot{q}_{d,j}^2 q_{d,j} dt\,,$	$B_{P,j} = \int_0^T 2f_j \dot{q}_{d,j}^2 dt\,,$ $D_{P,j} = \int_0^T \dot{q}_{d,j}^2 dt\,,$ $F_{P,j} = \int_0^T \dot{q}_{d,j}^2 q_{d,j}^2 dt\,.$

Table 1: Optimal parameters $\hat{K}$ and $\hat{q}_e$.

For the SEA case, the cost functional J_2 has a unique global minimum and hence, if such value is not admissible, then

$$\hat{K} = \begin{cases} K_m \text{ if } J_i(K_m) < J_i(K_M) \\ K_M \text{ if } J_i(K_M) < J_i(K_m)\,. \end{cases} \tag{49}$$

On the other hand, for cost functional J_1, the optimal stiffness value can be obtained solving (46) which has three solutions. Hence, the optimal stiffness can be one of these solutions or it can lie on the border of the admissible range of values.

For PEA, the performance index depends on the two optimization variables K and q_e. However, both cost functionals have a unique global minimum. Hence, if the optimal values are such that $\hat{K} \notin [K_m\ K_M]$ and/or $\hat{q}_e \notin [q_{e,m}\ q_{e,M}]$, then the optimal parameters are in the border of the admissible range of values. Consider the following cases:

1. if $\hat{K} \notin [K_m\ K_M]$ and $\hat{q}_e \in [q_{e,m}\ q_{e,M}]$. In this case, if $\frac{\partial J_{1,j}}{\partial K_j} = 0$ is satisfied by $\hat{q}_e$,
$$\hat{K} = \begin{cases} K_m \text{ if } J(K_m, \hat{q}_e(K_m)) < J(K_M, \hat{q}_e(K_M))\,, \\ K_M \text{ if } J(K_M, \hat{q}_e(K_M)) < J(K_m, \hat{q}_e(K_m))\,; \end{cases}$$

2. $\hat{K} \in [K_m\ K_M]$ and $\hat{q}_e \notin [q_{e,m} q_{e,M}]$. In this case, if $\frac{\partial J_{1,j}}{\partial q_{e,j}} = 0$ is satisfied by $\hat{K}$,
$$\hat{q}_e = \begin{cases} q_{e,m} \text{ if } J(\hat{K}(q_{e,m}), q_{e,m}) < J(\hat{K}(q_{e,M}), q_{e,M}) \\ q_{e,M} \text{ if } J(\hat{K}(q_{e,M}), q_{e,M}) < J(\hat{K}(q_{e,m}), q_{e,m})\,; \end{cases}$$

3. $\hat{K} \notin [K_m\ K_M]$ and $\hat{q}_e \notin [q_{e,m}\ q_{e,M}]$, then the optimal pair $\hat{K}$, $\hat{q}_e$ is related to the minimum value among the following: $J(K_m, q_{e,M})$, $J(K_M, q_{e,M})$, $J(K_m, q_{e,m})$ and $J(K_M, q_{e,m})$.

Remark 4 *In* (26)*, as well as in* (27)*,* (28)*, the stiffness is linear. Now, let us analyse the case in which the stiffness is nonlinear. In general, we can write the dynamics as a function of the nonlinear spring force as*

$$f(\ddot{q},\dot{q},q) = -\sigma(q-\theta) \tag{50}$$
$$\sigma(q-\theta) = (K_1(q-\theta) + K_2(q-\theta)^2 + \cdots + K_i(q-\theta)^i) \tag{51}$$

where $\sigma(q-\theta)$ is a generic monotonic function of the elongation.

For the SEA case, it holds

$$f(\ddot{q},\dot{q},q) = -\sum_{i=1}^{n} K_i(q-\theta)^i \tag{52}$$
$$J_m\ddot{\theta} = -\sum_{i=1}^{n} K_i(q-\theta)^i + \tau\,. \tag{53}$$

Similarly, for the PEA case it yields,

$$f(\ddot{q},\dot{q},q,t) = \sum_{i=1}^{n} K_i(q_e-q)^i + \tau\,. \tag{54}$$

Consider for example the following case, of a n-DoF system actuated by SEA, with $n=3$, and $K_1 = K_2 = 0$, $K_3 = K$, then replacing in (52) and (53), it yields

$$f(\ddot{q},\dot{q},q,t) = -K(q-\theta)^3 \tag{55}$$
$$J_m\ddot{\theta} = K(q-\theta)^3 + \tau\,, \tag{56}$$

and following the same procedure as presented before, we have

$$\begin{aligned}
\theta_j &= (K_j^{-1} f_j(\ddot{q}_d,\dot{q}_d,q_d,t))^{1/3} + q_{d,j}\,,\\
\dot{\theta}_j &= (K_j^{-1} f_j(\ddot{q}_d,\dot{q}_d,q_d,t))^{-2/3}\dot{f}_j(\ddot{q}_d,\dot{q}_d,q_d,t) + \dot{q}_{d,j}\,,\\
\ddot{\theta}_j &= (K_j^{-1} f_j(\ddot{q}_d,\dot{q}_d,q_d,t))^{-5/3}\dot{f}_j(\ddot{q}_d,\dot{q}_d,q_d,t) +\\
&\quad (K_j^{-1} f_j(\ddot{q}_d,\dot{q}_d,q_d,t))^{-2/3}\ddot{f}_j(\ddot{q}_d,\dot{q}_d,q_d,t) + \ddot{q}_{d,j}\,.
\end{aligned}$$

So, the torque to track the desired trajectories is

$$\begin{aligned}
\tau_j = J_{m_j}&(K_j^{-1} f_j(\ddot{q}_d,\dot{q}_d,q_d,t))^{-2/3}((K^{-1}\dot{f}_j(\ddot{q}_d,\dot{q}_d,q_d,t)) + \ddot{q}_{d,j} +\\
&(K_j^{-1} f_j(\ddot{q}_d,\dot{q}_d,q_d,t))^{-2/3}\ddot{f}_j(\ddot{q}_d,\dot{q}_d,q_d,t) + f_j(\ddot{q}_d,\dot{q}_d,q_d,t)\,.
\end{aligned}$$

In this way, we can obtain the expressions of the cost index, and we can still solve the problem for the nonlinear stiffness case, using suitable methods, e.g. numerical ones. ◇

3.3 Trajectory optimization problem

With the procedure followed so far, we can replace the optimal values of $\beta(q)$ in (38) and hence reformulate the problem in terms of the link trajectories $q(t)$ which

are now the only optimization variables. In other words, we have now the following simpler optimization problem:

$$\min_{\tau(t),q} J_i(q,\dot{q},\ddot{q}), \qquad i \in \{1,2\}$$
$$s.t. \begin{cases} \text{Dynamics equations} \\ q(t) = q(t+T) \\ \xi_1(q,\dot{q},\ddot{q}) \leq 0 \\ \xi_2(q,\dot{q},\ddot{q}) = 0 \end{cases} \tag{57}$$

In this paper we do not solve the new problem analytically, except for the One-DoF case. However, we provide a numerical solution to the trajectory optimization problem, applying our method to a Single Joint System and Two-Link manipulator.

Notice that the new optimization problem is not written in a conventional form, e.g. in a general Bolza form, as

$$\min_{u(t)} \Phi(x(t_f)) + \int_{t_0}^{t_f} L(x(t),u(t))dt$$
$$s.t. \begin{cases} \dot{x} = g(x(t),u(t)) \\ x(0) = x_0 \\ \chi_1(x) \leq 0 \\ \chi_2(x) = 0 \end{cases} \tag{58}$$

$\Phi(\cdot)$ and $L(\cdot)$ provide a mathematical representation of the objective function in terms of the states $x(t)$ and the control input $u(t)$; $g(\cdot)$ is a function of the system dynamics; x_0 denote the initial conditions for the states, and χ_1, χ_2 are the nonlinear constraints that define the task.

For example, let us consider the SEA case using the cost functional J_2. Replacing the coefficients $F_{S,j}$, $G_{S,j}$, $H_{S,j}$ and the optimal stiffness $\hat{K}_j$ (48), in the cost functional (47), it yields

$$\begin{aligned} J_{2,j} &= \frac{G_{S,j}^2}{4F_{S,j}} - \frac{G_{S,j}^2}{2F_{S,j}} + H_{S,j} \\ &= \frac{(\int_0^T (J_{m_j}\ddot{q}_{d,j} + f_j)^2 dt)^2}{4(\int_0^T (J_{m_j}\ddot{f}_j)^2 dt)} + \frac{2(\int_0^T (J_{m_j}\ddot{q}_{d,j} + f_j)^2 dt)}{\int_0^T (J_{m_j}\ddot{f}_j)^2 dt} \\ &+ \int_0^T 2J_{m_j}\ddot{f}_j(J_{m_j}\ddot{q}_{d,j} + f_j)dt\,, \end{aligned}$$

which is not in the form (58).

The optimization problem written in the Bolza form will be useful to solve the trajectory optimization problem using GPOPS-II [20]. To translate the problem in

a conventional form we propose the following steps, providing an example for the SEA case using the cost index J_2.

1. Write the actuated dynamics of the system as in (34), that can be expanded as
$$f = M(q)\ddot{q} + C(q,\dot{q})\dot{q} + K_v\dot{q} \tag{59}$$
which describes a planar manipulator, where $M(q)$, $C(q,\dot{q})$, K_v, are in order the inertia, coriolis and damping matrices; q, $\dot{q}$, $\ddot{q}$ are the link positions, velocities and accelerations, respectively.

2. Define the vector of state variables $x(t) \in \Re^m$, m is the number of state variables, which for the case of the example are
$$x(t) = [x_1(t)\,,\, x_2(t)\,,\, x_3(t)\,,\, x_4(t)\,,\, x_5(t)\,,\, x_6(t)]^T\,,$$
$$\begin{aligned} &x_1(t) = q(t)\,, \quad x_2(t) = \dot{q}(t)\,, \\ &x_3(t) = \mu(t)\,, \quad x_4(t) = \gamma(q,\dot{q},\varphi(q,\dot{q}))\,, \\ &x_5(t) = \rho(q,\dot{q},\varphi(q,\dot{q}))\,, \\ &x_6(t) = \hat{K}\,. \end{aligned}$$
Here $\varphi(q,\dot{q}) = M^{-1}(q)(C(q,\dot{q})\dot{q} + K_v\dot{q})$ denotes the inverse dynamics of the system described by (59). $\gamma(\cdot)$, $\rho(\cdot)$ are functions of this inverse dynamics. $\mu(t) = \int_0^T (J_m\ddot{f})^2$ is a function that corresponds to the term $F_{S,j}$, which is chosen to ease the problem solution; J_m the motor inertia.

3. Write the dynamics in state space as $\dot{x}(t) = g(x(t),u(t))\,,$
$$\begin{bmatrix} \dot{x}_1 \\ \dot{x}_2 \\ \dot{x}_3 \\ \dot{x}_4 \\ \dot{x}_5 \\ \dot{x}_6 \end{bmatrix} = \begin{bmatrix} x_2 \\ \varphi(\cdot) \\ (J_m\ddot{f})^2 \\ 2(J_m\ddot{f})(J_m x_3 + f) \\ (J_m x_3 + f)^2 \\ 0 \end{bmatrix} \tag{60}$$
where $\dot{f} = \frac{df}{dt}$, and $\ddot{f} = \frac{d\dot{f}}{dt}$

4. Write the cost functional (e.g. (47)) in terms of the state variables as
$$J_{2,j} = -\frac{x_4^2}{4x_3} + x_5 \tag{61}$$

For all cases considered, namely systems actuated by PEAs or by SEAs using indices J_1 or J_2, the same procedure can be followed according to the specific case, i.e. the states might be properly chosen and the formulation needs to be adapted to the dynamics of the system.

3.4 Examples of Stiffness and Pre-load optimization

In this section, we apply our methodology to two mechanical systems: a Single Joint System and a Two-Link Manipulator actuated either by SEA or by PEA. In both cases we report simulation results and in the first case we also address the analytical solution of the problem.

3.4.1 Single Joint System

Consider a Single Joint System, actuated by SEA or PEA, which performs a desired task. The dynamics of this mechanical system is

$$\begin{aligned} M\ddot{q} + c\dot{q} + mgL\cos q + K(q-\theta) &= 0 \\ J_m\ddot{\theta} + K(\theta - q) &= \tau \end{aligned} \tag{62}$$

in case of SEA, and

$$M\ddot{q} + c\dot{q} + mgL\cos q + K(q - q_e) = \tau \tag{63}$$

in case of PEA, where $M = mL^2 + I$, L is the length of the link, m is the load at the end of the link, I the inertia of the link and c is the damping. Let us assume that in both cases, the optimal link trajectory is given as $q_d(t) = B + A\sin(\omega t)$, where the amplitude A, the frequency ω, and the angle B around which the link oscillates, depend on the task.

In the PEAs case, the problem of finding optimal stiffness and pre-load can be solved analytically. Indeed, substituting $q_d(t)$, $\dot{q}_d(t)$ and $\ddot{q}_d(t)$ in (63), we can obtain τ that in turn can be substituted in J_1. The minimum of J_1 is achieved with

$$\begin{aligned} \hat{K} &= \omega^2 M + \frac{8mgLB_J(2,A)\sin B}{A^2} \\ \hat{q}_e &= B + \frac{2gmLAB_J(1,A)\cos B}{A^2\omega^2 M + 8mgLB_J(2,A)\sin B}, \end{aligned}$$

where $B_J(n,x)$ is the Bessel function. Notice that for small amplitudes, i.e. $A \to 0$, $\frac{8B_J(2,A)}{A^2} \to 1$, the optimal stiffness becomes $\hat{K} = \omega^2 M + mgL\sin B$ which corresponds to the resonant condition for the linearized system in $q = B$.

For the cost functional J_2, the minimum is obtained with

$$\begin{aligned} \hat{K} &= \omega^2 M + \frac{2mgLB_J(1,A)\sin B}{A} \\ \hat{q}_e &= B + \frac{AmgLB_J(0,A)\cos B}{A^2\omega^2 M + 2mgLB_J(1,A)\sin B}. \end{aligned}$$

Also in this case, for small amplitudes, the optimal stiffness becomes $\hat{K} = \omega^2 M + mgL\sin B$ which corresponds to the resonant condition for the linearized system in

$q = B$. Of course, for the nonlinear system, the cost function obtained by using the optimal parameters assumes a bigger value but $|\tau|$ achieves the minimum value. This is similar to the resonance concept of linear systems.

Finally, for a given B, the optimal values for $\hat{K}$ obtained by using J_1 and J_2 are quite similar. In particular, if $B = 0$ and for any amplitude A, $\hat{K} = \omega^2 M$, i.e. the value of stiffness corresponding to the resonant condition for the linearized system in $q = 0$.

In the SEAs case, the problem of finding optimal stiffness can be solved analytically only in case of cost functional J_2. Indeed, solving the first equation of (62) for θ and substituting it by its second derivative in the second equation of (62), we obtain τ, and substituting it in J_2, with $\dot{\theta}(t) = K^{-1}(M\ddot{q}_d(t) + c\dot{q}_d(t) + mgL\cos q_d(t)) + q_d(t)$, the minimum can be achieved in closed form, but for the sake of space, it is not reported here. However, in case of $B = 0$, $c = 0$ and for small amplitudes, the optimal value is

$$\hat{K} = \frac{MJ_m\omega^2}{(M + J_m)},$$

which corresponds to the resonant condition for the linearized system around $q = 0$, without losses ($c = 0$).

In case of J_1, the optimal stiffness and the corresponding value of the cost functional can be only obtained numerically. For a comparison between PEA and SEA in terms of efficiency, and to underline the advantage of soft w.r.t. stiff actuation, in Fig. 11 we report the cost saving in terms of J_1 and J_2 in case of PEAs or SEAs w.r.t. the stiff case. In particular, Fig. 11a and 11b show the energy saving using J_1 as measure. On the other hand, Fig. 11c and 11d show the energy saving using J_2 as measure.

In particular, considering Fig. 11a and 11c, the use of PEAs allows to get as much more saving as the amplitude and the frequency of the desired link trajectory decrease, independently from the cost functional used, i.e. J_1 or J_2. However, we have a consistent saving also in case of large values of frequency, independently from the amplitude.

Conversely, in case of SEA, savings depend on the cost functional that we consider. In terms of J_1, consistent savings can be obtained increasing the frequency. The amplitude influences significantly only for small values. In terms of J_2, consistent savings can be obtained for small values of amplitude and large values of frequency or for large values of amplitude and small values of frequency.

From another point of view, we can conclude that, in terms of J_2, PEA is more convenient for small amplitudes at low frequency or large amplitudes at high frequency, while SEA is more convenient for small amplitudes at high frequency or for large amplitudes at low frequency. In terms of J_1, we can observe differences

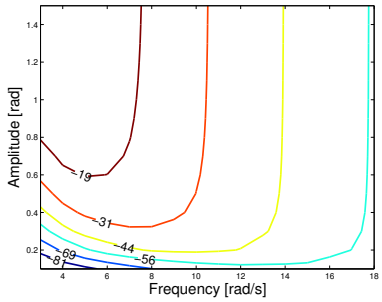

(a) Energy saving in terms of J_1 for PEAs.

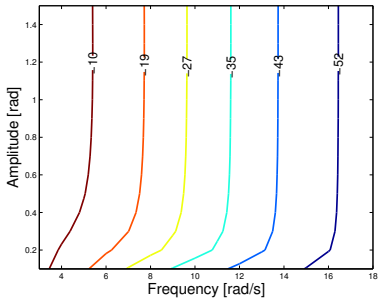

(b) Energy saving in terms of J_1 for SEAs.

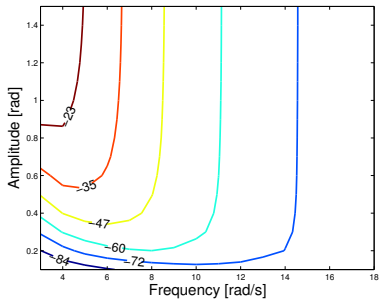

(c) Energy saving in terms of J_2 for PEAs.

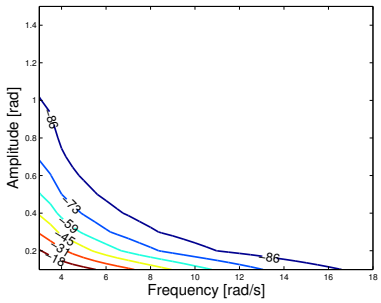

(d) Energy saving in terms of J_2 for SEAs.

Figure 11: Energy saving (in % w.r.t. the stiff case) for a single joint system, varying the amplitude A and the frequency ω of the desired joint trajectory $q_d(t) = A\sin(\omega t) + B$, with $B = 0$.

w.r.t. J_2 only in case of SEA. Indeed, SEA becomes convenient only for high frequencies, independently from the amplitude.

3.4.2 Two-Link Manipulator

Consider now a two-link manipulator actuated by SEAs, which is hence an underactuated system (2 motors and 4 DoF). For the given case, assume that $q_{1,d} = A_1\sin(\omega t) + B_1$ and $q_{2,d} = A_2\sin(\omega t) + B_2$ are the desired link trajectories. The robot performs a pick and place-like task on a horizontal plane, moving from a given initial position Q_1 to a given final position Q_2. The values of amplitudes A_1 and A_2, as well as of angle B_1 and B_2 around which each link moves, depend on Q_1 and Q_2. Of course, for any couple of points, these parameters are univocally determined by inverse kinematics.

For this example, we have performed several simulations applying our methodology. Some of them are reported in [21], where an analysis of cost functionals J_1

and J_2 in case of SEAs, as well as the optimal stiffness $\hat{K}$ for different values of frequency ω is provided. Moreover, the cost values J_1 and J_2 for the same tasks using different springs are also reported. According to simulation results and for the desired trajectories chosen, the optimization of the stiffness allows to save up to 62% of energy w.r.t. the rigid case.

One particular case is presented here as a general example of the overall results. For this case, the desired initial and final positions of the end effector in the task space are given by the cartesian points $Q_1 = (-13;5)$ and $Q_2 = (14;6)$ (in centimeters). The desired link trajectories calculated by inverse kinematics are assumed to be sinusoidal at a frequency $\omega = 4.5\ rad/s$ and the amplitudes and bias angles are respectively $A_1 = 0.45\ rad$, $B_1 = 1.5\ rad$, $A_2 = 1.5\ rad$, and $B_2 = 0.1\ rad$. Let us apply the method proposed to determine the optimal stiffness for each joint with respect to J_1. Table 2 shows the simulation results for the trial presented[3].

	Joint 1 $q_1 = 0.45\cos 4.5t + 1.5$	Joint 2 $q_2 = 1.5\cos 4.5t + 0.1$	TOTAL J_1
$\hat{K}\ [Nm/rad]$	0.2	0.09	
J_1	0.003	0.07	0.073
$K^*\ [Nm/rad]$	0.22	0.1	
J_1	0.003	0.075	0.078
$K_{min}\ [Nm/rad]$	0.05	0.05	
J_1	0.04	0.35	0.39
$K_{max}\ [Nm/rad]$	0.82	0.82	
J_1	0.07	0.1	0.17
Stiff	$K \to \infty$	$K \to \infty$	
J_1	0.09	0.1	0.19

Table 2: Simulation results for the trial presented. Cost index for different values of stiffness in a Two-Link robot

In Figs. 12a and 12b we show the simulation results for the two-link manipulator. The optimal value of stiffness is the one that generates the lowest cost. In this case, from the simulation we obtain $\hat{K}_1 = 0.2\ Nm/rad$ and $\hat{K}_2 = 0.09\ Nm/rad$. We observe that for lower values of stiffness the cost reaches a maximum value. This means that it is not worth to use softer actuators than the optimal. The simulation results presented here will be confronted with the experimental results in next sections. All the dynamic parameters used for the simulations are obtained from the model of the experimental two-link manipulator that will be described in the following.

[3] $\hat{K}$ is the optimal stiffness value determined from the simulations. K^* is the nearest elastic constant available for the implementation.

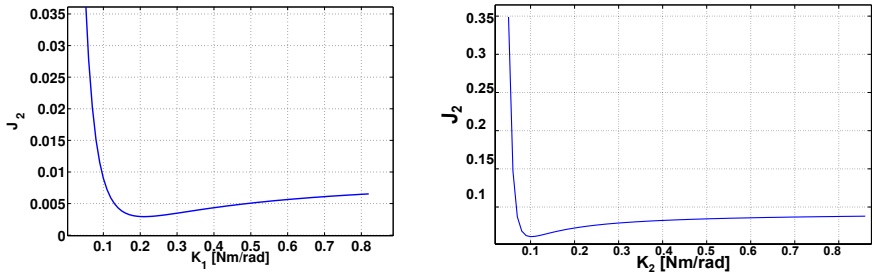

(a) Link 1 (b) Link 2

Figure 12: Simulation results for the two-link manipulator actuated by SEAs. Energy Cost J_2 for different values of stiffness K_1 and K_2. Parameters for simulation: Links Mass $m_1 = 0.34\ Kg$, $m_2 = 0.135\ Kg$, Links length $L_1 = L_2 = 0.1\ m$, Motor inertia $J_{m1} = J_{m2} = 10^{-5}\ Kgm^2$

3.5 Examples of Simultaneous Optimization of Stiffness and Link Trajectories

So far, we have described the analytical method to find the optimal parameters of a mechanical system actuated either by SEA or by PEA, given any desired trajectory. First, we have used sinusoidal link trajectories to prove that it is possible to optimize the actuation parameters and re-write the problem in terms of these trajectories that are now the only optimization variables. The problem in (57), after applying the methodology proposed, depends only on the trajectories. At this point, it is still an optimal control problem that can be solved, for instance, using nonlinear programming methods. Particularly, we use a general purpose optimal control software (General Pseudospectral Optimization control Software-GPOPS-II) to find the optimal trajectories.

As defined in [20], the optimization problem that will be solved using GPOPS-II is stated as detailed in the following.

1. Determine the desired task: for the example, a pick and place-like task to be executed with a Two-Link planar manipulator. Two points of interest are required; e.g. the starting (pick) point Q_s and the end (place) point Q_e of the end-effector, defined in the cartesian space.

2. Consider that the problem can be written in P phases, where P indicates a number of events for which one or more conditions may change. For the example, $P = 2$; the phases are defined by

   - Phase 1: the motions of the system to go from Q_s to Q_e in a time interval $[0, T_1]$.

   - Event: In the start and end points, joint velocity is zero.

- Phase 2: the motions of the system to go from Q_e to Q_s in a time interval $[T_1, T_2]$.

3. Write the cost function for each phase in terms of the state variables as in (61). In this case the cost function does not change for each phase.

4. Define the constraints for the desired task

   - Dynamic constraints, defined as $\dot{x}^{(p)} = a^{(p)}[x^{(p)}, u^{(p)}, t^{(p)}]$. For this problem the dynamics is defined as in (60).

   - Event constraints given by $b_{min} \leq b[x^{(p)}, u^{(p)}, t^{(p)}, s] \leq b_{max}$. For this problem, when the event occurs, i.e. the start or end points are achieved and the velocity of the joints becomes zero, all the states have the same value, which ensures that the trajectory is continuous.

   - Other constraints as inequality path constraints, defined as $c_{min} \leq c[x^{(p)}, u^{(p)}, t^{(p)}] \leq c_{max}$. or integral constraints defined as $q_{min}^{(p)} \leq q^{(p)} \leq q_{max}^{(p)}$. For this example, the minimum and maximum bounds that the states may achieve considering the physical characteristics of the system, and the desired initial and end points in the Cartesian space.

   Notice that the constraints defined here correspond to the constraints defined in (57).

The following examples consider the dynamics of a single joint system actuated either by SEA or PEA and a Two-Link Robot actuated by SEA. The first two cases, i.e. those for the single joint system, are illustrative and simple, and the results can be verified analytically. In the last case, we compare the cost when using the optimized trajectories with the cost when using sinusoidal trajectories as reported in table 2.

3.5.1 Single Joint System

Consider the Single Joint System, whose dynamics can be written as (62) if actuated by SEA and (63) for the PEA case. The constraints of the link trajectories are $q(0) = q(T) = 1$ *rad* and $q(T/2) = -1$ *rad* and the velocity constraints are $\dot{q}(0) = \dot{q}(T) = \dot{q}(T/2) = 0$ *rad*$/s$, with period $T = 2\pi$ *s*. We compare the results obtained from the numerical optimization and the expected results obtained analytically. The results of the optimal trajectory solution found for the Single Joint System are shown in Fig. 13a in the case of PEA and in Fig. 13b in the case of SEA. We observe that in this case the trajectories obtained are sinusoidal as expected and all the constraints are satisfied. Specifically, for both cases we expected an amplitude of $A = 1$ *rad* for a trajectory defined by $q_d(t) = A\cos\omega t$ which can be verified in the figures presented. Another example carried out using SEA is presented; for this, consider that the torque is $\tau = 0$ *Nm*, then $J_1 = 0$ and $J_2 = 0$. The

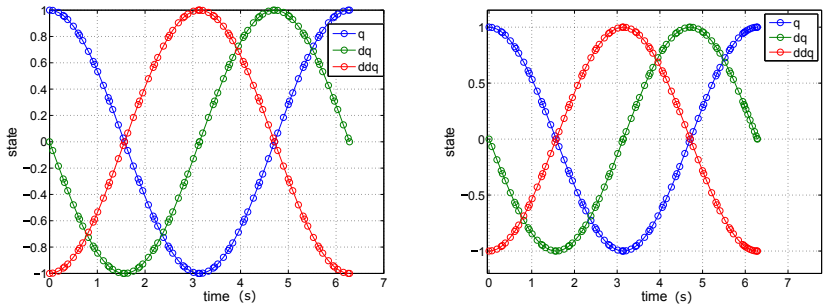

(a) PEA case (b) SEA case

Figure 13: Optimized trajectory one-DoF Manipulator actuated by PEA or by SEA. q is the position, dq is the velocity and ddq is the acceleration. For this example unitary masses and inertia are considered

optimal stiffness according to the analytical calculation is $\hat{K} = 0.5\ Nm/rad$, while from the optimization we find that $K = 0.53\ Nm/rad$. Moreover, the performance index obtained is $J_2 = 7.9 \times 10^{-8}$.

In the case of the manipulator actuated by PEA, the analytical value of the performance index is $J_2 = 2.1 \times 10^{-5}$ with a constant optimal stiffness of $\hat{K} = 1\ Nm/rad$. From the optimization we obtain $J_1 = 2.8 \times 10^{-5}$ and the stiffness corresponds to the expected value, i.e. $\hat{K} = 1\ Nm/rad$. For this case we have that the optimal pre-load is $\hat{q}_e = 0\ rad$.

3.5.2 Two-Link Manipulator

Now, let us analyze an example using a Two-Link Manipulator actuated by SEA, whose dynamics is given by (27) and (28). We define the desired cartesian points of start (Q_s) and end (Q_e) of a pick and place task and calculate the initial conditions of position and velocity for each joint to reach the desired points. Table 3 shows the parameters set for the example reported here.

Using the optimization software GPOPS-II, the optimal link trajectories $\hat{q}_1(t)$ and $\hat{q}_2(t)$ are obtained, as well as the optimal stiffness $\hat{K}_1$ and $\hat{K}_2$ such that they satisfy the constraints and minimize the cost functional $J_2 = J_{2,1} + J_{2,2}$. Figs. 14a and 14b show the resulting optimal trajectories for the desired task. Notice that the trajectories obtained are periodic, but they are not sinusoidal.

With the optimized trajectories and the optimal stiffness $\hat{K}_1 = 0.002\ Nm/rad$ and $\hat{K}_2 = 0.0001\ Nm/rad$, the cost is $J_2 = 3.5 \times 10^{-4}$. Using other trajectories rather than the optimal ones, e.g. sinusoidal trajectories that satisfy the constraints, we obtain $J_2 = 4.3 \times 10^{-4}$ with $\hat{K}_1 = 0.1\ Nm/rad$ and $\hat{K}_2 = 0.001\ Nm/rad$. This means that the optimization of the trajectories can further reduce the energy con-

Parameters	Value
$Q_s = (x_s, y_s)$ $Q_e = (x_s, y_s)$ Cartesian points in [cm]	(11.25, 6.9) (-10.17, 8.42)
$T\ [s]$	2π
Initial conditions	$q_1(0) = 1.4\ rad$, $q_2(0) = -1.7\ rad$
Constraints (Periodic Motions)	$q_1(T/2) = 1.6\ rad$, $q_2(T/2) = 1.7\ rad$ $q_j(0) = q_j(T)$ $\dot{q}_j(0) = \dot{q}_j(T) = \dot{q}_j(T/2) = 0\ rad/s$

Table 3: Parameters used for the example presented, emulating a pick and place task

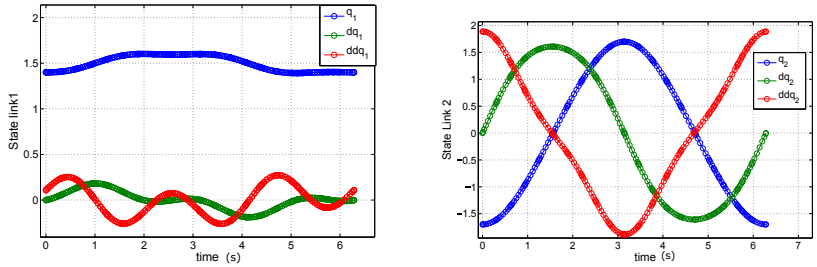

(a) Link 1 (b) Link 2

Figure 14: Optimized link trajectories for a two-Link SEA Manipulator. q is the position, dq is the velocity and ddq is the acceleration.

sumption. For this particular case, the reduction is of 20% w.r.t. the case when only the stiffness is optimized.

3.6 Experimental Results

To show the validity and the applicability of the methodology proposed, we report the results of experimental tests. First, we present a Single Joint System (hopping robot) actuated by a SEA. For this example we show that even though the proposed method is analytical, it is directly applicable to existing systems whose model is not accurate or not available at all. Moreover, we present the example of a Two-Link Robot actuated by SEA which performs a pick and place task. We report the results when using predefined cyclic trajectories, and we also carry out the optimization of link trajectories.

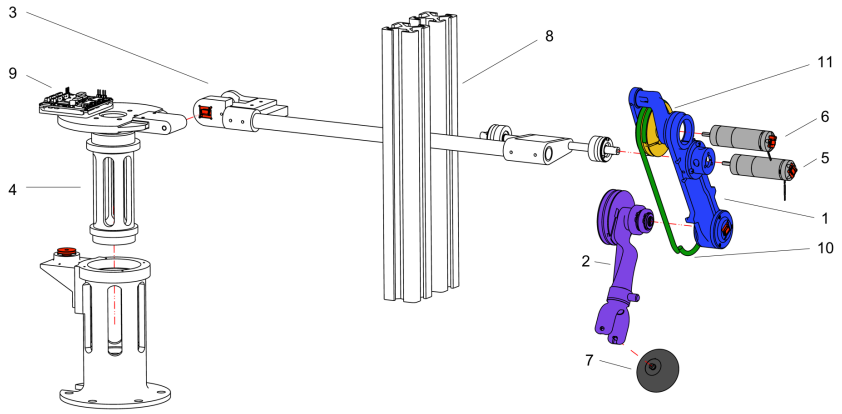

Figure 15: Exploded 3D view of the hopping robot. Torque and corresponding deformation used for stiffness identification are shown.

3.6.1 Model–Free Application: One-DoF hopping robot prototype

We report here an experimental application on a prototype of the hopping robot represented in Fig. 15. Indeed, the optimization of the actuation parameters requires to evaluate the function $f_a(\ddot{z},\dot{z},z,\ddot{q},\dot{q},q,t)$ in (30) in the case of SEA, or in (33) in the case of PEA, in terms of the desired link trajectories. However, in an experimental setup, $f_a(\cdot)$ can also be directly measured from the real system by means of suitable sensors. To carry out the optimization, the derivatives of the measured signal $f_a(t)$ are required. These signals can be obtained by applying estimation techniques, e.g. state reconstructor as in [22]. Hence, through the following experiment we are able to show that our method can be applied to systems whose model is unknown.

The following description refers entirely to Fig. 15 which shows that the robot has one leg composed by two links (1 and 2 in Fig. 15), three DoFs and it is linked to the frame through two non actuated DoFs (3 and 4 in Fig. 15). All joints are provided with a contactless magnetic rotary position sensor. The hopper is actuated by a SEA in the knee, while the other joint is stiff. The series elastic transmission (10 in Fig. 15) between the actuator (11 in Fig. 15) and the knee joint is composed of two rubber bands. A wheel (7 in Fig. 15) is placed at the extremity of the leg so the effect of the friction component perpendicular to the direction of motion is reduced. Vertical hopping is achieved by constraining the leg through a vertical linear guide (8 in Fig. 15). We acquire the measurements from the encoders and implement a proportional control scheme to provide the torque inputs to the motors which depend on the desired trajectories. This controller is fast enough to guarantee that the joint trajectories are the desired ones, as in the simulations.

The stiffness of the equivalent torsional spring between the knee link and the actu-

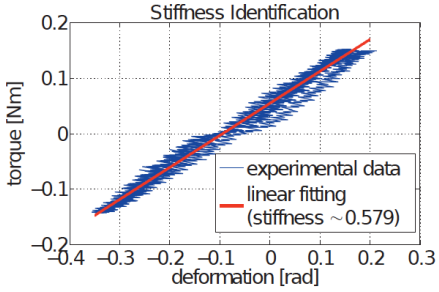

Figure 16: Torque and corresponding deformation used for stiffness identification.

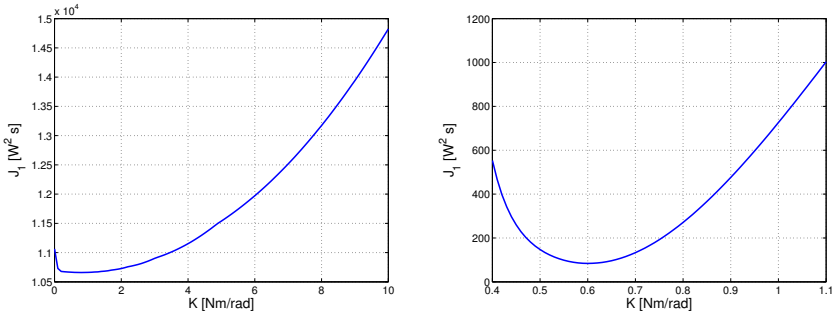

(a) Cost index J_1 for different values stiffness in case of PEAs.

(b) Cost index J_1 for different values stiffness in case of SEAs.

Figure 17: Cost indices J_1 for different values of K. In the PEA case, for each value of stiffness, the corresponding value of the cost functional is computed by using the best value of $\hat{q}_e$.

ator has been experimentally determined by applying different value of torques and the corresponding deformations (Fig. 16, Stiffness identification). Once the stiffness value is known (~ 0.58 Nm/rad), sinusoidal reference signals that guarantee a stable hopping have been imposed to the motors (black lines). During the experiment, we measured the hip and knee positions (red and blue lines), and hence the signal $f_a(t)$ in (30), or (33), in the SEA or PEA cases could be obtained straightforward. With these results, we verify that it is possible to apply our method to find the values of cost functionals J_1 and J_2 for different values of $\hat{K}$ and the corresponding best value of $\hat{q}_e$ in PEA case, as reported in Figs. 17 and 18. For both indices the best result in terms of energy saving can be obtained using SEAs by setting the stiffness to $K \approx 0.6$ Nm/rad.

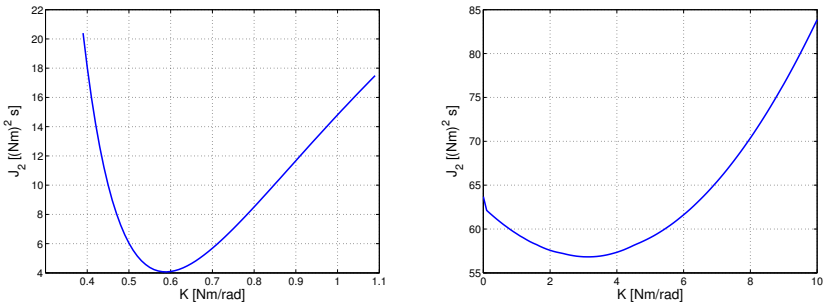

(a) Cost index J_2 for different values stiffness in case of SEAs.

(b) Cost index J_2 for different values stiffness in case of PEAs.

Figure 18: Cost indices J_2 for different values of K. In the PEA case, for each value of stiffness, the corresponding value of the cost functional is computed by using the best value of $\hat{q}_e$.

3.6.2 Two-Link Manipulator

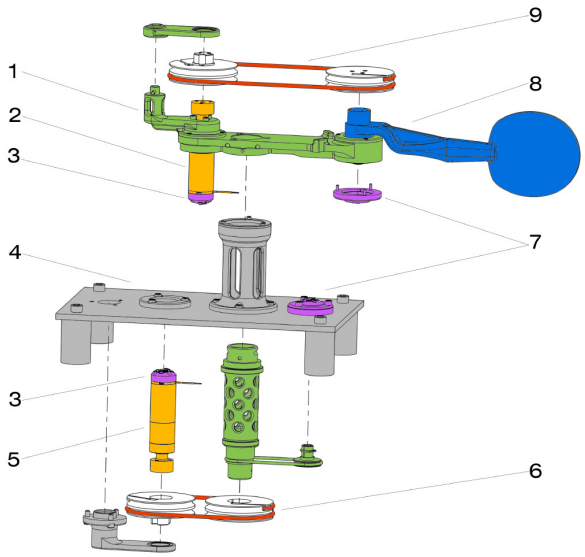

Figure 19: Prototype of the 2 DoF Manipulator actuated by SEA

3.6.3 System Description

The prototype of the manipulator is represented in Fig. 19. It is an underactuated arm with two links (8 in Fig. 19) and two joints (2, 5 in Fig. 19), connected by a mechanism of pulleys (6 in Fig. 19) and series elastic transmissions (rubber

bands (9 in Fig. 19)) between the actuators and the joints. Either the joints and the links are provided with contactless magnetic rotary position sensors AS5045[4] (3, 7 in Fig. 19). Additionally, hall effect analog current sensors ACS714[5] have been placed in series to each motor in order to measure the current consumption during the task. An electronic board[6] is used to acquire the measurements from the encoders and the current sensors, and to implement a closed loop position control scheme to track the desired trajectories. For the reported study, there is no control loop to track the link trajectories. All the position measurements acquired from the sensors have been filtered using a butterworth lowpass filter, with cutoff frequency $\omega_c = 15\ rad/s$ to reduce noise effects.

Index calculation
The current measurements I, sampled each 5 ms were used to calculate the torques as $\tau_I = K_I I$, where $K_I = 18.4\ mN/A$ as specified in the motors specifications [7]. Therefore, the cost indices, $J_1 = \sum_j \int_{t_0}^{t_0+T} (\tau_j \dot{\theta}_j)^2 dt$ and $J_2 = \sum_j \int_{t_0}^{t_0+T} \tau_j^2 dt$ can be calculated. Moreover, as the root mean square value of the current (I_{RMS}) helps to understand the energy consumption of each joint of the manipulator, we additionally calculate it as

$$I_{RMS_j} = \sqrt{\frac{1}{T}\left(\int_{t_0}^{t_0+T} I_j^2(t)dt\right)}, \tag{64}$$

which as previously mentioned is strictly related to the cost indices used and provides a measure of the real energy consumption to broaden the analyses presented. To implement the I_{RMS} function, the current measurements are squared and then filtered using a butterworth lowpass filter with cutoff frequency $\omega_c = 2\ rad/s$.

3.6.4 Test Protocol and Procedure

Applying the methodology proposed, we determine the optimal spring constant for each joint. To implement the optimal stiffness, we characterize different elastic elements (series elastic transmissions) using a Materials Testing Machine [8]. Thus, we obtain the curve of the force vs. the displacement $F = -k\Delta(x)$ for each elastic sample. The elastic elements used are approximately linear, so we can calculate the elastic constant k (in N/m). Fig. 20a shows the characteristic curve of one of the elastic rubbers. The length of the rubber band sample in the curve shown is $L = 16\ cm$. A constant force at a constant speed is applied to elongate it up to 2 cm, and the cycle is repeated several times for each trial. With a linear regression method we obtain $k = 640\ N/m$. Fig. 20b shows the characteristic curve of the

[4] http://www.ams.com

[5] http://www.pololu.com/file/0J196/ACS714-Datasheet.pdf

[6] http://www.naturalmotioninitiative.com/

[7] maxon DCX 22S. http://dcx.maxonmotor.com with graphite brushes 24 V, and planetary gearhead GPX22 with reduction ratio 186 : 1, 5 and 6

[8] Zwick Roell Z005

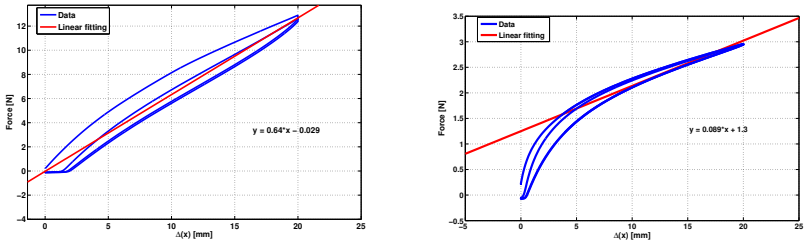

(a) Characteristic curve of an elastic element.

(b) Characteristic curve of a soft elastic element.

Figure 20: Characteristic curves of force vs. displacement of elastic elements.

softest elastic used. Notice that the curve has a linear region, which is considered for the analysis; although the rubber bands characteristic is assumed approximately linear, nonlinearities exist and must be taken into account for experiments.

The pulleys of the platform allow to change the linear elastic constant into the corresponding torsional elastic constant: $K = kr^2$ (in Nm/rad), where r is the pulley radius. For instance, with a pulley of $r = 3\ cm$, the torsional elastic constant for the sample presented is $K = 0.57\ Nm/rad$. Using different pulley radius and different elastic elements, we can have different spring values as well. Notice that the torsional constants can be calculated with high accuracy. The error of the fitting model, as in Figs. 20a or in 20b has been considered in the worst case. The error in determining the linear constant, i.e. the difference between the model and the real data is $k \pm 62N/m$. On the other hand, the radius of the pulleys that have been printed in a 3D printer[9] with an accuracy of $r \pm 1\ mm$. So, the torsional springs can be determined with an accuracy of $K \pm 6 \times 10^{-5}\ Nm/rad$. However, the available values depend on the materials and on the pulleys used. Based on these calculations, for the implementation we consider $\hat{K} \pm 10\%$. The differences between the costs when using the optimal theoretical and the implemented values of stiffness do not change significantly in simulation (around 1 % as shown in table 2). For the experiments carried out, we have used five different rubber bands and pulleys of two different radius ($r = 2\ cm$ and $r = 3\ cm$).
The experiments have been carried out to accomplish a repetitive task, as a pick and place, where the end effector goes cyclically from one initial position Q_1 to a certain final position Q_2, which are defined previously. There are two interesting cases for this study that will be considered, namely predefined link trajectories to accomplish the desired task, and optimized link trajectories.

[9] Stratasys Dimension Elite

3.6.5 Stiffness optimization of a Two-DoF manipulator with pre-defined trajectory

Consider now the case of stiffness optimization of the Two-link manipulator with pre-defined trajectory. Assume a simple case of cyclic trajectory, defined for each link as

$$q_j = A_j \cos \omega t + B_j \,,$$

where the frequency ω can be chosen according to the system specifications, and the amplitude A_j and offset angle B_j, as well as the input to the motors, i.e. θ_j, are properly calculated through inverse kinematics, considering the elastic element between the actuator and the link.

Recall the simulation results reported in section 3.4, which are used to generate the experimental trials reported in this section. For the particular case, the desired initial and end points of the pick and place task, as well as the desired trajectories are the ones presented in the simulation results in table 2.The use of elastic actuation was analyzed in 4 cases (considering the physically implementable elastic transmissions): first, using the implemented optimal spring values ($K_j^* = \hat{K}_j \pm 10\%$) for each joint $K_1^* = 0.22\ Nm/rad$ and $K_2^* = 0.1\ Nm/rad$, calculated through the methodology presented; second, with softer springs than the optimal for each joint $K_{1_{soft}} = 0.08\ Nm/rad$, $K_{2_{soft}} = 0.06\ Nm/rad$; third, using an elastic element stiffer than the optimal one, $K_{1_{stiff}} = 0.57\ Nm/rad$, $K_{2_{stiff}} = 0.35\ Nm/rad$, and finally the rigid case. In all the studied cases, we verify that the desired joint trajectories (θ) are followed properly. Figs. 21a and 21b show that the measured joint position green line) tracks the desired joint trajectory given to the motor (represented in blue) with a mean error of 0.1%. All the calculations have been done considering the steady state of the system. The analysis of the initial pick consumption and transient is not in the scope of this work.

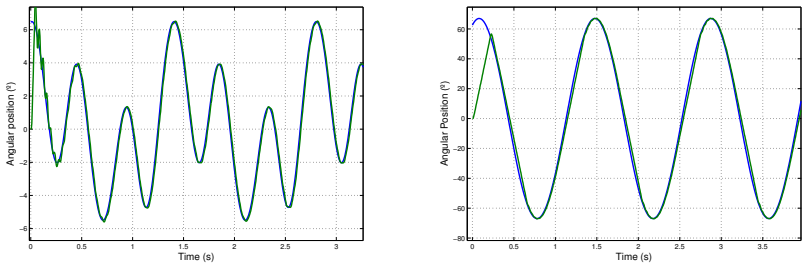

(a) Joint 1 (b) Joint 2

Figure 21: Manipulator Joints trajectory tracking

Furthermore, to ensure that the task performed is the same in all the compared cases, we verify the behavior of the corresponding link trajectories. Beyond having similar link angular positions, the comparison is done between the corresponding

initial and end desired positions of the end effector Q_1 and Q_2 for each case of analysis, i.e. the task is accomplished. Table. 4 shows the distance between the experimental and the desired values of the initial and end positions for the same desired link trajectories using different stiffness values, namely optimal, softer than the optimal, stiffer than the optimal, and rigid.

	$\hat{K}$	$K < \hat{K}$	$K > \hat{K}$	Rigid
$J_{1_{TOTAL}}$	0.1542	0.7964	0.3154	0.5672
$I_{RMS_{Total}}$ (A_{rms})	1.37	2.95	1.79	1.68
K_1 [Nm/rad]	0.2	0.08	0.57	Rigid
K_2 [Nm/rad]	0.1	0.06	0.35	Rigid
Distance to Q_1 [cm]	2.8	1.9	1.1	0.9
Distance to Q_2 [cm]	3.6	1.0	1.1	0.3

Table 4: Results: Index and current consumption for each stiffness case for one cycle of the pick and place task. Distance from the desired Initial $Q_1 = (-13,5)$ and end $Q_2 = (14,6)$ points of the pick and place task for each case of actuation

The trajectory of the end effector during the experiment is shown in Fig. 22. Notice that the initial and end points are repeatable for each case, even if there are differences with the desired trajectory. Then, Figs. 23a and 23b show the measured link

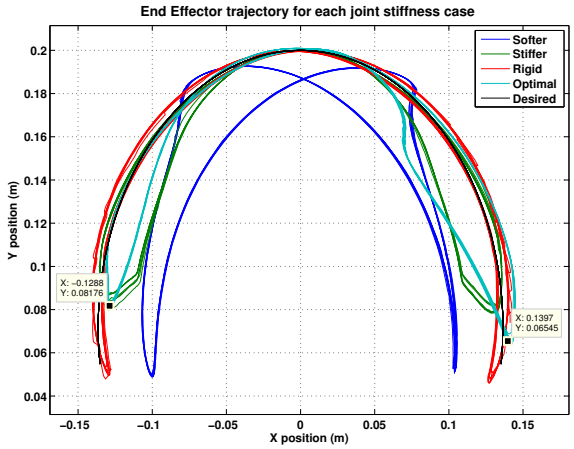

Figure 22: End effector behavior for each case of stiffness

positions q_1 and q_2 respectively for the four cases of stiffness analyzed. Observe that the softest elastic, particularly in Link 2 produces higher angular position errors and a delay. Notice that in Fig. 20b, the characteristic curve of the softest elastic used is linear only in a region and it has been considered linear for this experiment. The angular positions of Link 2 in the other cases (optimal spring, stiffer spring and rigid actuation) behave as expected. Instead, there are bigger differences

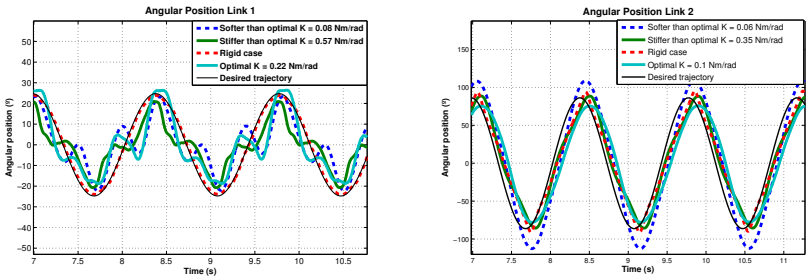

(a) Link 1 (b) Link 2

Figure 23: Compared link positions for the same desired task

in the position of Link 1 with respect to the desired behavior. The differences in the measured link positions are mainly due to nonlinearities, non-modeled dynamics and uncertainties in the model.

The I_{RMS} value of each joint provides additional information to analyze the energy consumption and it is strictly related to the cost indices. We have observed that with the optimal joint stiffness the I_{RMS} is always lower than for the rest of the cases, proving that lower energy consumptions can be obtained with the optimization of actuation parameters. Moreover, the stiff transmission is not always the worst case in terms of energy consumption, taking into account the I_{RMS}. For example, Figs.24a and 24b, show that with the optimal joint stiffness, the current requirement accumulated for each joint during the task is lower than for the rest of the actuation cases, while the softer case is the most expensive one. Table 4 summarizes the cost

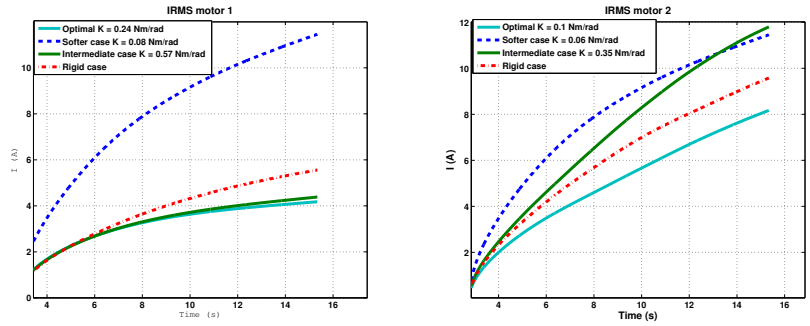

(a) Joint 1 (b) Joint 2

Figure 24: Manipulator IRMS

results for the presented case, where the savings when using the optimal springs, in terms of J_1 are at least 58% w.r.t. a stiffer case and 79% w.r.t. the rigid case. The values in Table 4 are calculated from the measurements, notice that the trend is the same as expected from the simulations. As the data depend on the sensors, the accuracy of the index depends directly on the sensors accuracy, which for the

encoders is $\theta \pm 0.002$ *rad*, and for the current sensors is $I \pm$ 1 *mA*. In terms of the cost, the calculation is again highly accurate, i.e. $J_1 \pm 2 \times 10^{-6}$.

In general, a significant energy saving is achieved when optimizing the actuation parameters. In the following, We present some consolidated results from a set of experiments. We carried out 320 trials of the same task using different elastic transmissions and different trajectories at different frequencies as summarized in Table 5. Fig. 25 shows the costs of this repetitive task when using the optimal stiffness rather that softer, stiffer or rigid actuation. We chose different desired

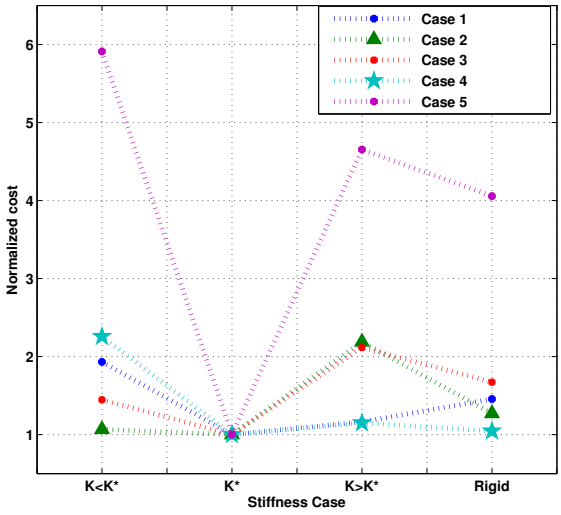

Figure 25: Performance of optimal actuation

trajectories at different frequencies from the 320 trials performed, as summarized in Table 5. In each case, the cost of the task is calculated when the system has reached the steady state. For the analysis, the cost J is normalized in every case with respect to the cost of when using the optimal actuation parameters, such that for the latter, the normalized cost is $J_n = 1$. Furthermore, notice that for all the other cases of stiffness, the cost is always higher than when optimizing the stiffness. Depending on the frequency and on the amplitude of the desired trajectories, the optimized stiffness allows energy savings up to 79%.

3.6.6 Simultaneous optimization of joint trajectories and stiffness of a Two-link manipulator with SEAs

Herein we present the case of simultaneous optimization of joint trajectories and stiffness of a Two-link manipulator with SEAs. In this part, the results reported correspond to of a set of experiments carried out to test the optimal trajectories and

Case	q_1 [rad]	$q_2[rad]$
1	$A_1 = 0.31$ $B_1 = 1$ $\omega_1 = 1rad/s$	$A_2 = 1.7$ $B_2 = 0.04$ $\omega_2 = 1rad/s$
2	$A_1 = 0.1$ $B_1 = 1.5$ $\omega_1 = 2rad/s$	$A_2 = 1.6$ $B_2 = 0.01$ $\omega_2 = 2rad/s$
3	$A_1 = 0.5$ $B_1 = 1$ $\omega_1 = 3.5rad/s$	$A_2 = 1.6$ $B_2 = 0.03$ $\omega_2 = 3.5rad/s$
4	$A_1 = 0.05$ $B_1 = 1.6$ $\omega_1 = 4rad/s$	$A_2 = 1.5$ $B_2 = 0$ $\omega_2 = 4rad/s$
5	$A_1 = 0.25$ $B_1 = 1.5$ $\omega_1 = 4.5rad/s$	$A_2 = 1.7$ $B_2 = 0.1$ $\omega_2 = 4.5rad/s$

Table 5: Different cases of link trajectories q_1 and q_2 used to report Fig. 25.

stiffness found by solving the problem with GPOPS-II as described in section 3.5. In order to compare the results with the previous case of predefined trajectories, the conditions of the experiments are the same; the initial and end points (Q_1; Q_2) of the task are the ones chosen before. The desired states of the links are shown in Figs. 27a and 27b. The optimal joint stiffness for this example is $\hat{K}_1 = 0.12Nm/rad$ and $\hat{K}_2 = 0.05Nm/rad$. Recall results on Table 4. Now, Table. 6 shows the distance between the experimental and the desired values of the initial and end positions when using the optimal stiffness and optimal joint trajectories. On the other hand, regarding the cost index, observe that the mean square value of the current spent is $I_{RMS_{Total}} = 1.09\ A_{rms}$ and the index $J_1 = 0.12$ which is approximately a 20% lower consumption than the optimal case when using a pre-defined sinusoidal trajectory, under the same conditions.

	with $\hat{q}_j$ and $\hat{K}$
$J_{2_{TOTAL}}$ $I_{RMS_{Total}}$ (A_{rms})	0.0004 1.09
K_1 [Nm/rad]	0.12
K_2 [Nm/rad]	0.05
Distance to Q_1 [cm]	1.02
Distance to Q_2 [cm]	1.8

Table 6: Results: Index and current consumption for one cycle of the pick and place task.

Moreover, the trajectory of the end effector during the experiment is shown in Fig. 26. Observe that the desired initial and end points are reachable and the task is repeatable.

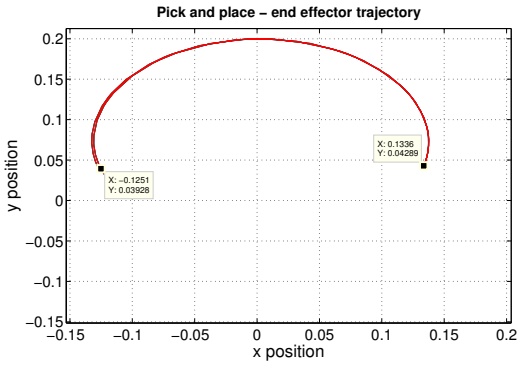

Figure 26: End effector behavior

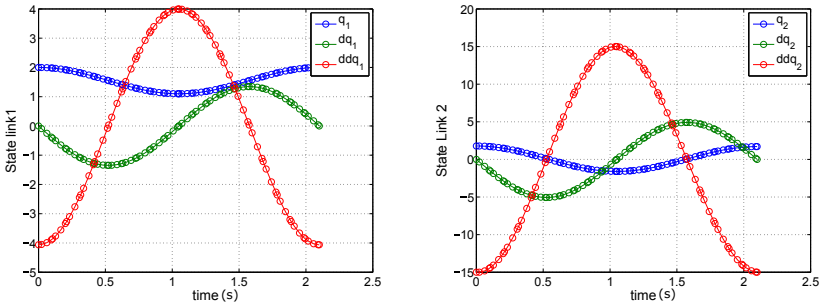

(a) Link 1 (b) Link 2

Figure 27: Optimization of trajectories: Desired States for manipulator's Links

Figs. 28a and 28b we show that the joint tracks the angular position and achieves a steady state. Figs. 29a and 29b show the measured link positions q_1 and q_2 respectively compared to the desired trajectories given by the optimization process in GPOPS-II. Due to the nonlinear behavior of the elastic elements, particularly the one of Link 1, the angular position presents a periodic error. However, the behavior of the system in terms of the initial and end points of the end-effector is not affected, achieving the task.

3.7 Conclusions

Energy efficiency is an important issue in robotics autonomous systems. In this paper, we have presented a methodology to analyze the role of soft actuators in the

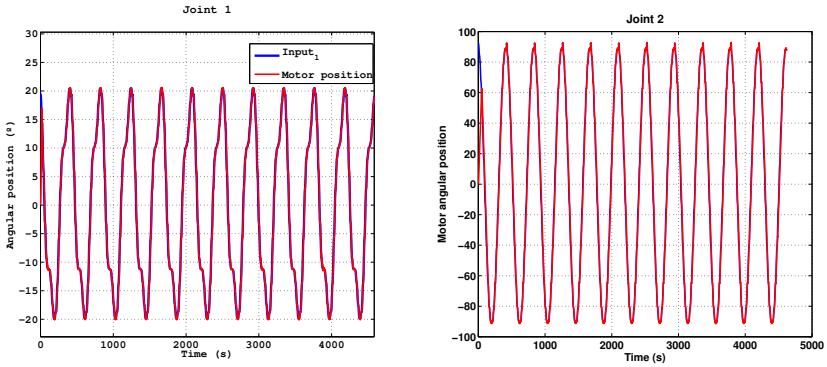

(a) Joint 1 (b) Joint 2

Figure 28: Joints angular positions measured vs. desired

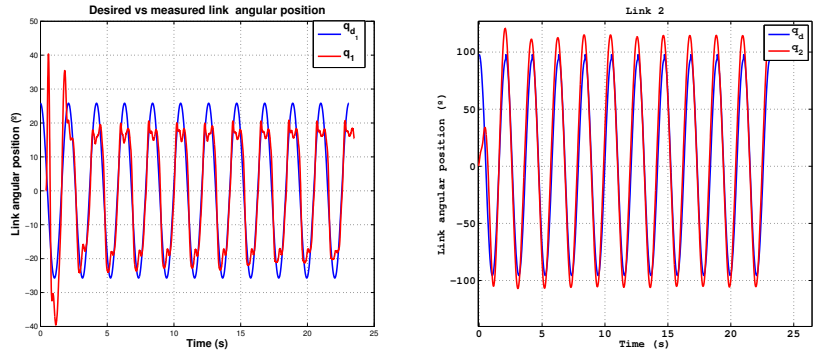

(a) Link 1 (b) Link 2

Figure 29: Links angular positions measured vs. desired

reduction of energy consumption of mechanical systems. As a consequence, we propose an analytical solution to find the optimal actuation parameters of n-DoF mechanical systems actuated by SEA or by PEA. The trajectories to accomplish a task play also an important role in the performance of mechanical systems. However, the actuation parameters and the trajectories are highly coupled. To solve this problem, we have the optimization problem in a simpler one that regards only the link trajectories.

Several simulations and some experimental tests were carried out to show the validity of the proposed methodology. A complete analysis that compares the energy cost of robotic systems that perform required tasks as a pick and place task or locomotion has been carried out. The strength point of our work is the fact of decoupling the complex problem of concurrently optimizing the actuation parameters and the actuation parameters, providing an analytical solution to the optimization problem. We are also able to show that using the optimal actuation parameters the

savings obtained go up to 62% and further savings of at least 20% are obtained when optimizing simultaneously the actuation parameters and the link trajectories.

4 Anticipaotory Control for Soft Robots

There are two main factors that enable humans to perform a wide variety of tasks in the real world: the musculoskeletal system and the Nervous System (NS). On the artificial side, while Soft Robots have been designed to reproduce some of the key features of the musculoskeletal system, from the control point of view, current approaches are still far from achieving performances comparable with those obtained by the NS. In this work, we present a novel control algorithm based on iterative control, which exhibits a typical human feature: learning an anticipatory action. The algorithm provides a *plug-and-play* control technique for Soft Robots that preserves their dynamic behavior. At the same time, it can be successfully applied to serial and parallel structures, while being robust against model uncertainties as well as different external force vector fields. Experiments show the effectiveness of the here proposed techniques.

4.1 Soft Robots & Anticipatory Behavior

In this section we introduce the model of Soft Robots and the concept of *anticipatory behavior*, i.e. a way to control such systems maintaining their mechanical characteristics.

Here we make the assumptions that the motor dynamics is negligible, and that the spring characteristic depends on the deflection, i.e. the difference between actual and reference position, and on an additional parameter useful e.g. to adjust the joint stiffness. The resulting model for a N-dof robot is:

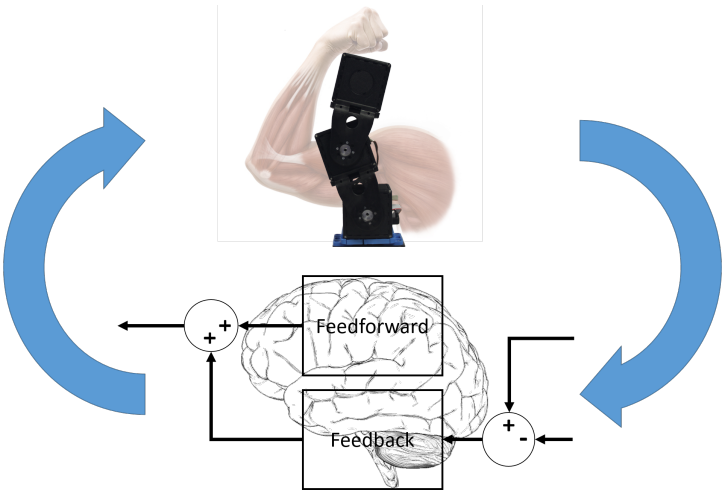

Figure 30: A control algorithm for Soft Robots: taking inspiration from how the NS deals with muscoloskeletal system.

$$M(q)\ddot{q} + C(q,\dot{q})\dot{q} + G(q) + T(q-r,d) = 0 \tag{65}$$

where $q \in \mathbb{R}^N$, $\dot{q} \in \mathbb{R}^N$, $\ddot{q} \in \mathbb{R}^N$ are the vectors of generalized joint positions, velocities and accelerations respectively, $M(q) \in \mathbb{R}^{NxN}$ is the inertia matrix and $C(q,\dot{q}) \in \mathbb{R}^{NxN}$ is the centrifugal and Coriolis matrix, $G(q) \in \mathbb{R}^N$ is the potential vector field, and $T(q-r,d) \in \mathbb{R}^N$ is the vector field representing the elastic torques. The control input is $r \in \mathbb{R}^N$, i.e. the reference position, and the stiffness input vector is $d \in \mathbb{R}^N$. $T(q-r,d)$ depends on the physical implementation of the elastic transmission. Joint stiffness is defined as the derivative of actuation torque w.r.t. the Lagrangian variables $\frac{\partial T}{\partial q}$. For the sake of clarity, we will omit the input d when not strictly necessary, and use the notation $T(q-r)$, meaning that the conditions stated have to be valid for every d.

In the majority of cases compliant elements are deliberately introduced in Soft Robot design to confer to the system additional characteristics like robustness, energy efficiency, and adaptability to cite a few. Hence control algorithms that preserve the mechanism stiffness are preferable w.r.t. approaches that deeply change the behavior of the system.

We can formalize this idea requiring the stiffness in closed loop to be in a neighborhood of radius δ of the open loop stiffness along the system trajectory ($q = r$), i.e.:

$$\left|\left|\frac{\partial T(q-r)}{\partial q}\Big|_{q\equiv r} - \frac{\partial T(q-\psi(q))}{\partial q}\Big|_{q\equiv\bar{q}}\right|\right| < \delta \qquad \bar{q}|\psi(\bar{q}) = \bar{q} \tag{66}$$

where the term on the left is the Euclidean matrix norm. Defining $DT_i(\cdot) \triangleq \frac{\partial \tau_i}{\partial q_i}(\cdot)$, and using the equation in appendix A (for the sake of simplicity we hypothesize here the diagonal dominance) we obtain:

$$2\left|\left|DT_i(0)\frac{\partial \psi_i(q)}{\partial q_i}|_{q\equiv\bar{q}}\right|\right| < \delta \tag{67}$$

Which means that, to preserve the mechanical stiffness characteristic, the proportional component of the feedback has to be sufficiently small, i.e.:

$$\left|\left|\frac{\partial \psi_i(q)}{\partial q_i}|_{q\equiv\bar{q}}\right|\right| < \frac{\delta}{2||DT_i(0)||} \tag{68}$$

On the other hand, feedforward action does not affect this condition, since it does not depend on q.

In human motor control, the term *anticipatory behavior* [23] refers to the preference to work mostly on feedforward (which can be learned through the repetitions of the same task [24]). In the robotic context this concept translates in reducing the proportional feedback control component.

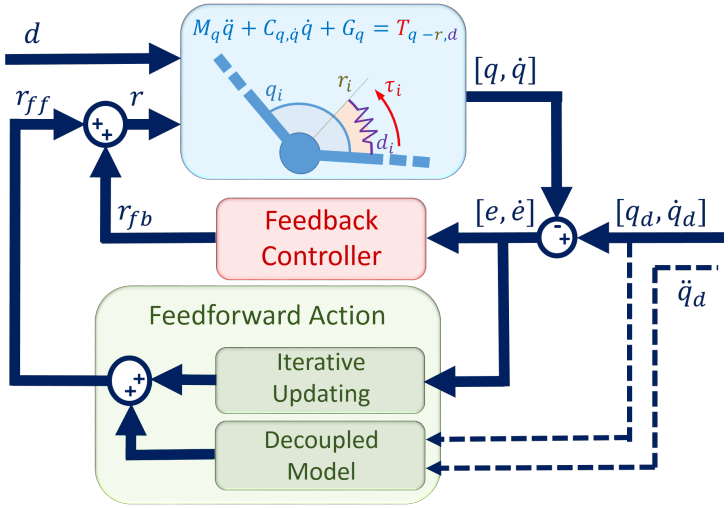

Figure 31: Schematic representation of the control architecture, with major quantities underlined. $[q,\dot{q}]$ are the Lagrangian variables, and q_d, $\dot{q}_d$, $\ddot{q}_d$ their desired evolutions. $[e,\dot{e}]$ is the tracking error. M, C and G are the inertia, centrifugal and potential field terms, T is the spring torques vector, d and r are the stiffness and reference inputs. r_{fb} is the feedback action, and r_{ff} is the feedforward action, which is the sum of a term precomputed and a term estimated.

4.2 Control Architecture

The scheme represented in Fig. 31 shows the overall control algorithm that combines a TVLQR feedback action and a feedforward component relying on a partial knowledge of the model and on an iterative updating law. Within the Control Theory, the ILC [25] provides a suitable framework to synthesize controllers in which a pure feedback loop and an iterative feedback loop concur to determine the input evolution. A generic ILC control law is:

$$r^{k+1}(t) = r^k(t) + c(e^k, e^{k+1}, t) \tag{69}$$

where k is the iteration index, $r^k(t) \in \mathbb{R}^N$ is the input vector at k-th iteration, $e^k \in \mathbb{R}^N$ is the error vector at k-th iteration and $c(e^k, e^{k+1}, t)$ is the *updating law*.

A general updating law is expressed by the sum of two terms

$$c(e^k, e^{k+1}, t) = ILC_{off}(t, e^k) + ILC_{on}(t, e^{k+1}), \tag{70}$$

where, in a full state proportional ILC, it is:

$$\begin{cases} ILC_{off}(t,k) = \mathbb{K}_{off}(t) \begin{bmatrix} q_d(t) - q^k(t) \\ \dot{q}_d(t) - \dot{q}^k(t) \end{bmatrix} \\ ILC_{on}(t,k+1) = \mathbb{K}_{on}(t) \begin{bmatrix} q_d(t) - q^{k+1}(t) \\ \dot{q}_d(t) - \dot{q}^{k+1}(t) \end{bmatrix} \end{cases}, \tag{71}$$

where $\mathbb{K}_{off}(t) \in \mathbb{R}^{Nx2N}$ and $\mathbb{K}_{on}(t) \in \mathbb{R}^{Nx2N}$ are the control gain matrices.

4.3 Decentralized Approach

In order to develop a control system as general as possible we adopt a decentralized approach (as seen e.g. in [26]). To this aim it is convenient to express the Soft Robot model 65 in a decoupled way:

$$\dot{x}(t) = Fx(t) + G\tau_i(q_i(t), r_i(t)) + D(t)\,, \tag{72}$$

where $x(t) = \begin{bmatrix} q_i & \dot{q}_i \end{bmatrix}^T$ is the state vector, τ_i is the i-th element of T, $r_i(t)$ is the i-th element of $r(t)$, while F, G and D have the form:

$$F = \begin{bmatrix} 0 & 1 \\ 0 & \dfrac{-\beta_i}{I_i} \end{bmatrix},\ G = \begin{bmatrix} 0 \\ \dfrac{1}{I_i} \end{bmatrix},\ D = \begin{bmatrix} 0 \\ \Delta_i + \eta_i(t) \end{bmatrix}. \tag{73}$$

Where I_i and β_i are, respectively, the inertia and the damping seen from the i-th joint, D is the vector of disturbs, modelled as the sum of a constant external force Δ_i and a time variant action $\eta_i(t)$ such that $\eta_i(0) = 0$, which contains also the neglected coupling actions (for further details refer to [26] Section 8.3).

In order to implement a decentralized controller, the control gains assume the following form:

$$\mathbb{K}_{off}(t) = \left[\text{diag}(K_{poff,i}) \,|\, \text{diag}(K_{doff,i})\right] \tag{74}$$

$$\mathbb{K}_{on}(t) = \left[\text{diag}(K_{pon,i}) \,|\, \text{diag}(K_{don,i})\right], \tag{75}$$

where $K_{poff,i} \in \mathbb{R}$ and $K_{doff,i} \in \mathbb{R}$ are the iterative control gains proportional to the position and velocity error of the i-th, respectively; and $K_{pon,i} \in \mathbb{R}$ and $K_{don,i} \in \mathbb{R}$ are the feedback control gains proportional to the position and velocity error, respectively. It is useful to define the vectors $K_{off,i} = [K_{poff,i} \quad K_{doff,i}]$ and $K_{on,i} = [K_{pon,i} \quad K_{don,i}]$.

Both a feedback control and a nominal feedforward action can be designed based on the model reported in (72). In addition the ILC will provide the suitable action for compensating $\eta_i(t)$ as reported in section 4.6.

Constant disturbances Δ_i can be compensated by either ILC or by a proper constant input action obtained before starting the learning phase.

4.4 Linearization

Given a reference trajectory $x_d(t) = \begin{bmatrix} q_{d_i}(t) & \dot{q}_{d_i}(t) \end{bmatrix}^T$, a nominal control action r_i^0 is derived by numerically solving $0 = Fx_d(t) + G\tau_i(q_{d_i}(t), r_i^0(t)) + \begin{bmatrix} 0 & \Delta_i \end{bmatrix}^T$. It is now possible to linearize the known dynamics of the system (72) (i.e. $\tau_i(q_i, r_i)$) around the desired trajectory $(x_d(t), r_i^0(t))$, obtaining:

$$\dot{x}(t) = A(t)x(t) + B(t)r_i(t) + W(t). \tag{76}$$

where

$$A(t) = \begin{bmatrix} 0 & 1 \\ \frac{1}{I_i}\frac{\partial \tau_i}{\partial q_i}(t) & \frac{-\beta_i}{I_i} \end{bmatrix}, \; B(t) = \begin{bmatrix} 0 \\ \frac{1}{I_i}\frac{\partial \tau_i}{\partial r_i}(t) \end{bmatrix}, \; W(t) = \begin{bmatrix} 0 \\ \eta_i(t) \end{bmatrix}. \tag{77}$$

4.5 Stability Analysis

The feedback action can be designed by the solution of the time varying linear quadratic optimization problem (see [27] Chapter 5):

$$J = \frac{1}{2}\int_0^{t_{fin}} (x^T Q(t) x + r_i^T R(t) r_i)\, \mathrm{d}t, \tag{78}$$

where $Q(t) \in \mathbb{R}^{2x2}$ is a positive semidefinite matrix and $R(t) \in \mathbb{R}^+$. The i-th feedback gain vector is given by:

$$K_{on,i}(t) = R(t)^{-1} B(t)^T S(t), \tag{79}$$

where $S(t)$ comes from the solution of the time-varying differential matrix Riccati equation:

$$\dot{S}(t) = -S(t)A(t) - A(t)^T S(t) + S(t)B(t)R(t)^{-1}B(t)^T S(t) - Q(t), \tag{80}$$

with the boundary constraint $S(t_{fin}) = \emptyset$.

4.6 ILC Convergence Analysis

An ILC convergence condition for a class of dynamic systems including (76), given in [28], results:

$$\rho([I + K_{on,i}(t)B(t)]^{-1}[I - K_{off,i}(t)B(t)]) < 1. \quad \forall t \in [0, t_{fin}] \;, \tag{81}$$

where $\rho(\cdot)$ represents the spectral radius.

Note that the (81) does not depend on $Ax(t)$ neither on $\eta_i(t)$, hence the proposed ILC updating law allows to compensate for the effects given by the not modeled dynamics.

Since the argument of the spectral radius in (81) is a scalar, $\rho(\cdot)$ is coincident with the absolute value. Hence by substituting the (79) in the (81) we obtain the following condition

$$\left| \frac{1 - K_{off,i}(t)B(t)}{1 + R(t)^{-1}B(t)^T S(t) B(t)} \right| < 1, \tag{82}$$

to be fulfilled. By rewriting:

$$K_{off,i}(t) = (1+\alpha_i(t))B(t)^{\dagger} + \Gamma_i(t), \tag{83}$$

where $B(t)^{\dagger}$ represents the Moore-Penrose pseudoinverse of the matrix $B(t)$, with $\alpha_i(t) \in \mathbb{R}$ and $\Gamma_i(t) \in \ker\{B(t)\}$ two functions to be chosen, we obtain the following convergence condition:

$$|\alpha_i(t)| < |1 + R(t)^{-1}B(t)^T S(t)B(t)| \quad \forall t \in [0, t_{fin}]. \tag{84}$$

A possible choice is:

$$\alpha_i(t) = \varepsilon\,(1 + R(t)^{-1}B(t)^T S(t)B(t)), \tag{85}$$

where $\varepsilon \in [0,1)$ is a parameter to be chosen considering the trade off between fast convergence and control cost. We heuristically found that for our experimental setup a good choice is $\varepsilon = 0.9$. Since $\Gamma_i(t) \in \ker\{B(t)\}$, from the (77) it follows that $\Gamma_i(t) = [K_{poff,i} \quad 0]$. Theoretically any choice of $K_{poff,i}$ would work, practically we achieved good performance by setting its value such that the following condition holds:

$$K_{poff,i}(t) = \frac{\int_0^{t_{fin}} K_{pon,i}(t)}{\int_0^{t_{fin}} K_{don,i}(t)} K_{doff,i}(t) \tag{86}$$

Finally, it is worth to notice that two quantities remain to be tuned: $Q(t)$ and $R(t)$. In the experimental tests we describe in the following section we chose $Q(t) = \mathrm{diag}([1,0])$ because the accuracy of the position measurements was much higher than the velocity ones. $R(t)$ has been left as a free parameter for the user to tune the controller authority.

4.7 Experimental Results

This section presents some application examples (hereinafter referred to as Experiment 1, Experiment 2, Experiment 3, and Experiment 4) of the proposed algorithm with various robot architectures: serial and parallel structures with a different number of dofs and configurations (for further details see the attached videos). The experiments were performed using the *qbmove maker pro* [29] (hereinafter simply referred to as qbmoves) actuators as testbed. These are modular variable stiffness servos based on an agonist-antagonist mechanism. For this actuator, the model of τ_i in (72) is:

$$\tau_i = 2k\cosh(ad_i)\sinh(a(q_i - r_i)) + m(q_i - r_i) \tag{87}$$

where τ_i, d_i, r_i and q_i are respectively the i-th component of T, d, r and q defined above, while $a = 6.7328$ [1/rad], $k = 0.0222$ [Nm] and $m = 0.5$ [Nm/rad] are model parameters.
These experiments aim to show:

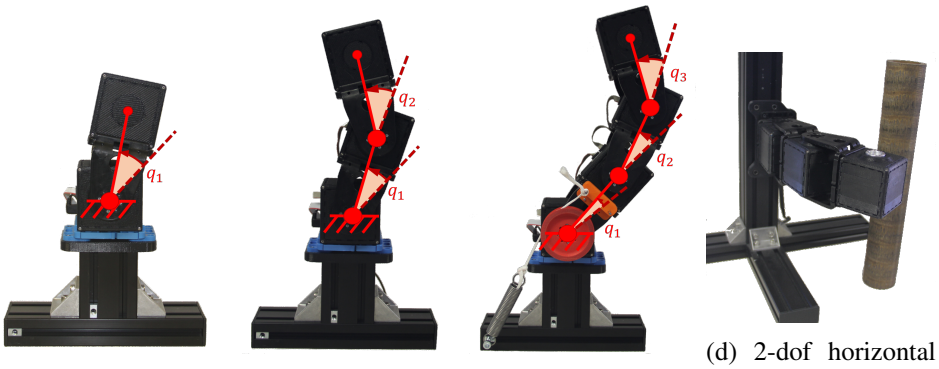

(a) 1-dof config. (b) 2-dof config. (c) 3-dof config. (d) 2-dof horizontal config.

Figure 32: Experimental setups and reference frames. 1-dof configuration (Experiment 1, and 2; 4.7.1, 4.7.2) (32a). 2-dof configuration (Experiment 1; 4.7.1) (32b). 3-dof configuration (Experiment 1; 4.7.1) (32c): a parallel spring is included in this setup to avoid that the torque required to the base actuator exceeds its torque limit. Notice that for the success of the experiment the knowledge of the exact elastic constant of the spring is not required. 2-dof horizontal configuration (Experiment 3; 4.7.3) (32d).

- the scalability of the method (Experiment 1, and 4);
- its ability to work with variable stiffness and in presence of uncertainties (e.g. a sign change of the gravity torque) (Experiment 1, 2, and 4);
- the *plug & play* behavior of the method, its high generality, and its model independence (no knowledge about the overall system dynamic and kinematic is required) (Experiment 1, and 4);
- the ability of a mostly feedforward control not to alter the stiffness characteristic of the system (Experiment 3).

Notice that the latter requirement is important to fully take advantage of the mechanical design of soft robotic systems that are able to mechanically vary their impedance, thus exhibiting a human muscle-like behavior.
Moreover, in order to remain as independent as possible from a given system architecture, the quantities β_i and I_i were estimated trough step response in the first phase of each experiment.

4.7.1 Experiment 1

Experimental Setup: In this experiment we considered three different setups, which consisted of serial chains of one, two and three qbmoves as shown in Fig. 32. We

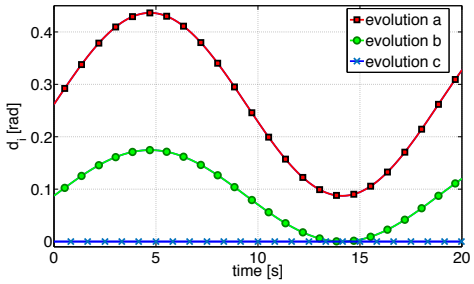

Figure 33: Stiffness input (d_i) evolution over time for the three different setups. Evolution 'a' is the one of the first qbmove for 1-dof case (see Fig. 32a), of the second qbmove for 2-dof case (see Fig. 32b) and for the third qbmove for 3-dof case (see Fig. 32c). Evolution 'b' is the one of the first qbmove for the 2-dof case and for the second qbmove for 3-dof case. Evolution 'c' is the one of the first qbmove for the 3-dof case.

chose:

$$q_1(t) = -\frac{\pi}{12}\cos(2t), \quad t \in [0,20] \tag{88}$$

as the desired trajectory for the first joint. The others joints follow a trajectory that is in phase opposition w.r.t. the one followed by the previous joint in the chain. The experiments were conducted with a time-varying stiffness different for each qbmove; Fig. 33 shows the stiffness input d_i for each joint for the three setups. The value for $R(t)$ was chosen to be constant and equals to 3. Such value was heuristically identified as a trade off between the ILC converge velocity and the control cost.
Results: Fig. 34a shows the evolution of the error integral over the iterations normalized by the terminal time (in this case $t_{fin} = 20$ s) and the number of joints for the three setups. For each system configuration the error reduction is greater than 60% w.r.t. the starting error. Fig. 34b shows that, iteration after iteration, the feedforward component becomes larger and larger w.r.t. the feedback component.

The minimum error can be observed for the 3-dof case. This is due to the fact that stiffness increases with the deflection, which depends on the wrench. At higher deflection, static friction and hysteresis become negligible and the spring model is more accurate.

4.7.2 Experiment 2

Experimental Setup: As reported in 4.2, we decomposed the uncertainties in $\eta_i(t)$ and Δ_i but we pre-evaluate only the Δ_i component. Due this fact, a major change in $\eta_i(t)$ (e.g. a change in sign of the gravity torque) is particularly challenging

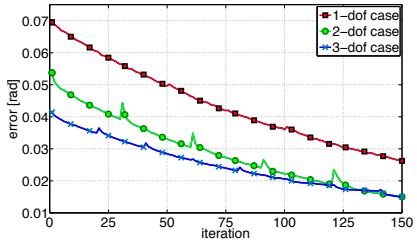

(a) Evolution of the error integral over the iterations normalized by the the terminal time and the number of joints for the three setups.

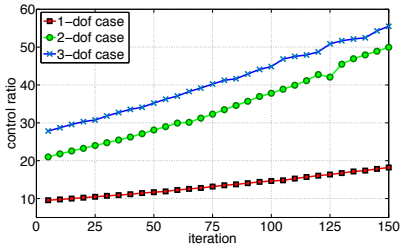

(b) Ratio between the integrals of the feedforward and feedback actions during the task for the three setups.

Figure 34: Effect of the ILC algorithm on the error integral 34a and anticipatory action 34b.

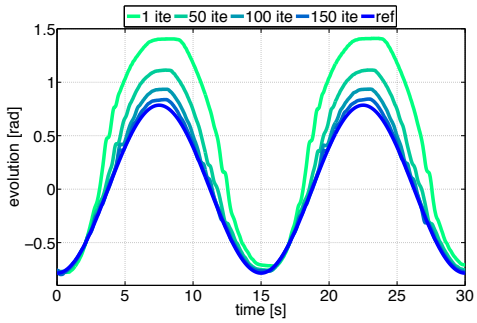

Figure 35: Trajectory evolution over the iterations for the experiment with low stiffness.

for the proposed method. This experiment aims to test the effectiveness of the ILC algorithm also in this limit condition. To do this, we imposed that the robot, depicted in Fig. 32a and already used in Experiment 1, must follow the following trajectory:

$$q_1(t) = -\frac{\pi}{4}\cos(\frac{4\pi}{30}t) + \frac{\pi}{4}, \quad t \in [0,30] \tag{89}$$

around the dashed line depicted in Fig. 32a. In this experiment we used $R(t)$ constant and equals to 1.

Results: Fig. 36 represents the reduction of the error integral normalized by the terminal time over the iterations with low, medium and high constant stiffness. Fig. 35 shows the time evolution of the link trajectory in four meaningful iterations for the low stiffness case, which exhibits the largest initial error. Results shown that in 150 iterations the desired trajectory is tracked with an error reduction about 95% w.r.t. the initial error for the low stiffness case.

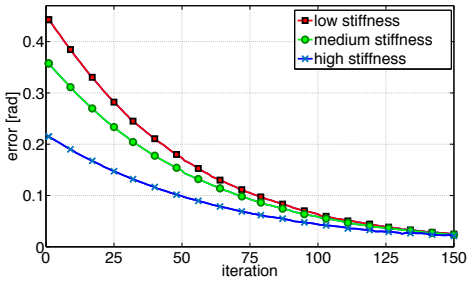

Figure 36: Evolution of the error integral over the iterations normalized by the terminal time for three different constant input stiffness values: $d_i = 0$, $d_i = 0.17$, $d_i = 0.44$ [rad], for the low, medium, and high stiffness case respectively.

4.7.3 Experiment 3

Experimental Setup: In this experiment we used the setup depicted in Fig. 32d. We ran the ILC algorithm to teach the robot to follow the desired trajectory on the horizontal plane both with low and high constant stiffness. Then, we placed a brass bar next to the robot in such a way that the impact was unavoidable. In this experiment we used $R(t)$ constant and equals to 2.
Results: As shown in Fig. 37 when the stiffness was low the robot could not move the bar. On the contrary when the stiffness was high the robot dropped the bar and continued following the trajectory. Fig. 38 shows the trajectory followed in both the experiments: at 0.94 s (magenta dashed vertical line) the robot impacts the bar. In the low stiffness case (Fig. 38a) the robot softly adapts to the external environment while in the high stiffness case (Fig. 38b) the robot at 1.3 s (orange dashed vertical line) drops the bar and converges to the desired trajectory in about 3 s (for the sake of readability we report the time evolution till 2 s).

4.7.4 Experiment 4

Experimental Setup: In this experiment we use a 3-dof Delta robot (see Fig. 39) composed of three joints connected to the end-effector through a parallel structure [30].

First of all, manually moving the end-effector, we taught to the robot the desired trajectory: a rest-to-rest task trough two obstacles (Obstacle 1, Obstacle 2), each consisting of two aluminum columns (Fig. 39). We taught the robot to pass trough Obstacle 1 and to jump over Obstacle 2. The input stiffness profile is time varying: the robot is stiff during the positioning over the target (points Target 1 and Target 2 marked as red dots) so that the precision is improved, and soft during the obstacles passing phases to be adaptable to the external environment. In this experiment we used $R(t)$ constant and equals to 3.

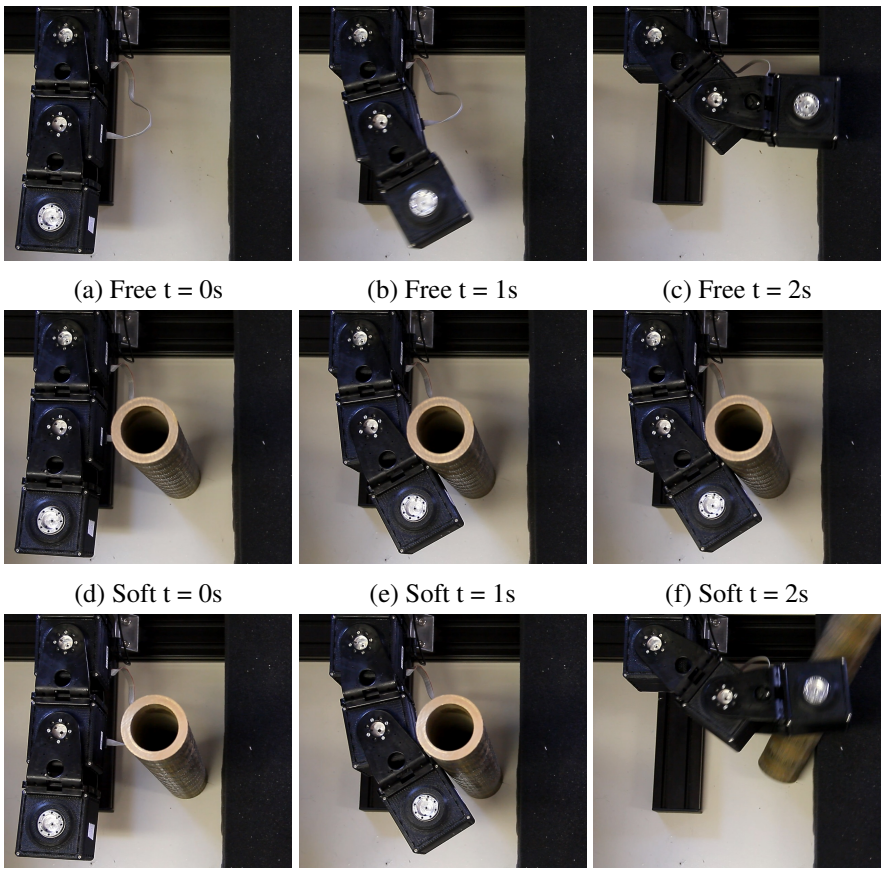

(a) Free t = 0s (b) Free t = 1s (c) Free t = 2s

(d) Soft t = 0s (e) Soft t = 1s (f) Soft t = 2s

(g) Stiff t = 0s (h) Stiff t = 1s (i) Stiff t = 2s

Figure 37: Robot positions at t = 0, 1 and 2 s for different stiffness input values. (a-c): Robot positions with no obstacle. (d-f): Robot positions with obstacle and low stiffness; the robot adapts to the external environment. (g-i): Robot positions with obstacle and high stiffness; the robot drops the bar.

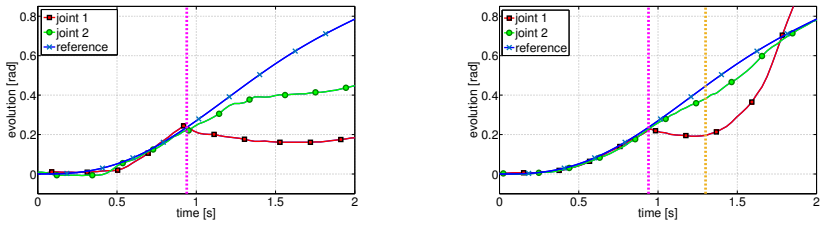

(a) Low stiffness input $d_i = 0$ rad (b) High stiffness input $d_i = 0.52$ rad

Figure 38: Trajectory followed by a 2-dof horizontal robot in presence of an obstacle. The impact occurs at 0.94 s. Low stiffness configuration 38a: the robot adapts to the external environment. High stiffness configuration 38b: the robot drops the bar at 1.3 s and continues to follow the desired trajectory.

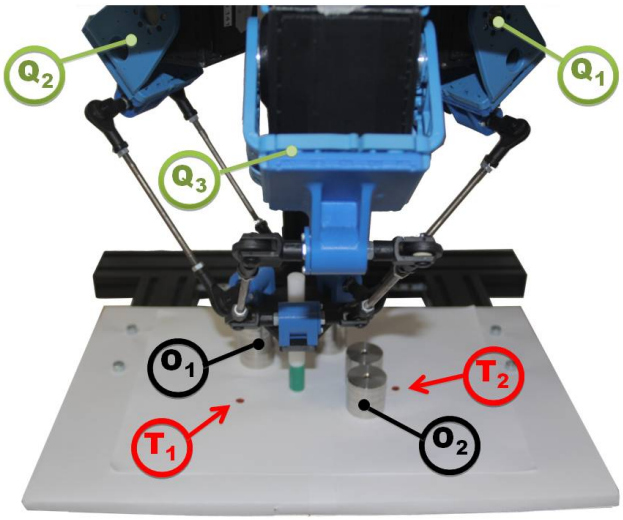

Figure 39: Delta robot used for the rest-to-rest experiment from T1 (Target 1) to T2 (Target 2). The red dots represent the target spots while the aluminum columns represent the obstacles (O1 Obstacles 1, O2 Obstacles 2). The robot has to move its end-effector between the columns of the Obstacle 1 and has to jump over Obstacle 2. Q1, Q2 and Q3 are the three actuators.

Result: Fig. 41 shows the trajectory following improvement between the first and the last iteration. Initially the robot could neither pass through the columns nor jump over the barricade failing to fulfill the task. At the end of the learning process the robot was able to successfully accomplish the task. Fig. 40 shows the error evolution over iterations. We can note that at 87-th iteration the error drops significantly. This is due to the fact that the robot learns how to pass through the second obstacle, improving the trajectory tracking.

4.8 Conclusions and Future Works

Some of the features of human motor control could be the key to advance the control state of the art in soft robotics. In this work, we presente an algorithm that combines a feedback component (TVLQR) and a feedforward action, through ILC, showing a human-like behavior: the learning of an anticipatory action, i.e. the growing authority of the feedforward action w.r.t. the feedback one, via task repetition. The here proposed control has been successfully applied to a soft robotic system that exhibits characteristics similar to the human musculoskeletal apparatus, in various configurations, degrees of freedom and tasks. Results show the effectiveness of the here proposed techniques in dealing with different kinematic structures, working conditions and external force fields. At the same time, the

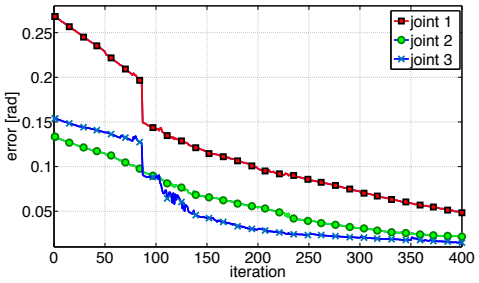

Figure 40: Evolution of the error integral over the iterations normalized by the the terminal time for the three joints of the Delta robot. At iteration 87 and 106 there are two drops of the error since the robot learned how to pass the Obstacle 2 and Obstacle 1, respectively. Not that the drop at 87th iteration is much higher than the drop at iteration 106.

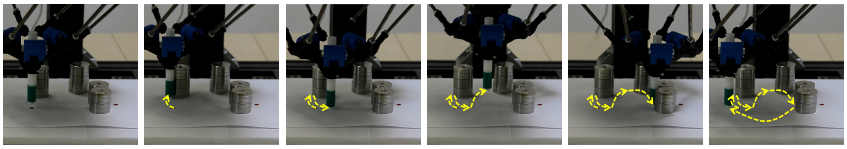

(a) 1st iteration: starting point. (b) 1st iteration: first obstacle passing. (c) 1st iteration: positioning for the jump. (d) 1st iteration: jump phase. (e) 1st iteration: place phase. (f) 1st iteration: returning phase.

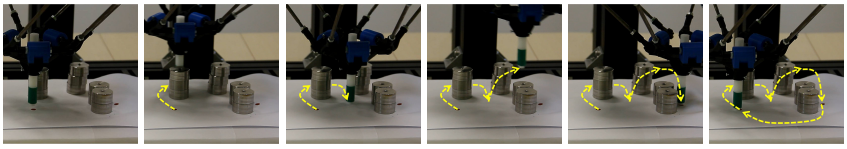

(g) 400th iteration: starting point. (h) 400th iteration: first obstacle passing. (i) 400th iteration: positioning for the jump. (j) 400th iteration: jump phase. (k) 400th iteration: place phase. (l) 400th iteration: returning phase.

Figure 41: First and last iteration photo sequence of the Delta experiment. (a, g): The robot should stand over the red dot (Target 1). (b, h): The robot has to pass through the two columns of Obstacle 1. In the first iteration it can not do it and it collides with one of the columns. (c, i): The robot prepares itself to jump over the second obstacle. (d, j): the robot has to jump over the obstacle. In the first iteration it jumps too early and fails. (e, k): The robot should position itself over the second target. In the first iteration, since it failed the jump, the robot stops against the obstacle. (f, l): The robot returns to the starting position.

methods described in this paper have been proven to be able to fully take advantage of the soft/stiff mechanical behavior of soft robots for task accomplishment. Given its *plug & play* and device independent behavior, the control paradigm can be easily extended to different robotic architectures. Future works will focus on further investigating these techniques, to approach problems both in motor control, with humans, and motion control, with robots.

APPENDIX A

In this section we report the demonstration of the inequality:

$$|a_{i,i}| < \frac{\delta}{2} \; \forall i \in \{1 \dots n\} \Rightarrow ||A||_2 \leq \delta \tag{90}$$

Where $A \in \mathbb{R}^{n \times n}$ is a matrix with diagonal dominance and $a_{i,j}$ is its element $\{i, j\}$. Considering the $2-$norm of A we have that:

$$||A||_2 = \max_i |\lambda_i| \tag{91}$$

Where λ_i are the eigenvalues of A. For the Gerschgorin Theorem we have that, if a system has diagonal dominance:

$$\max_i\{|\lambda_i|\} \leq \max_i\{|a_{i,i}| + \sum_{i \neq j} |a_{i,j}|\} \leq \max_i\{2|a_{i,i}|\} \tag{92}$$

Hence, considering that from the hypothesis derives directly that $\max_i\{2|a_{i,i}|\} < \delta$, from (91) and (92) the (90) is obtained.

The thesis can also be proved for many matrix norms, considering the existing matrix norms inequalities (e.g. $||A||_1 < \sqrt{n}||A||_2$, $||A||_\infty < \sqrt{n}||A||_2$, $||A||_F < Rank(A)\,||A||_2$)

References

[1] G. A. Pratt and M. Williamson, "Series elastics actuators," in *IROS*, 1995, pp. 399–406.

[2] B. Vanderborght, A. Albu-Schaeffer, A. Bicchi, E. Burdet, D. G. Caldwell, R. Carloni, M. G. Catalano, O. Eiberger, W. Friedl, G. Ganesh, M. Garabini, M. Grebenstein, G. Grioli, S. Haddadin, H. Hoppner, A. Jafari, M. Laffranchi, D. Lefeber, F. Petit, S. Stramigioli, N. G. Tsagarakis, M. V. Damme, R. V. Ham, L. C. Visser, and S. Wolf, "Variable impedance actuators: a review," *Robotics and Autonomous Systems*, vol. 61, p. 1601–1614, 12/2013 2013. [Online]. Available: http://www.sciencedirect.com/science/article/pii/S0921889013001188

[3] N. Tsagarakis, M. Laffranchi, B. Vanderborght, and D. Caldwell, "A compact soft actuator unit for small scale human friendly robots," *IEEE International Conference on Robotics and Automation*, vol. 1-7, pp. 1998–2004, 2009.

[4] A. Bicchi and G. Tonietti, "Fast and soft arm tactics: Dealing with the safety-performance tradeoff in robot arms design and control," *IEEE Robotics and Automation Magazine*, vol. 11, no. 2, June 2004.

[5] S. Haddadin, M. Weis, S. Wolf, and A. Albu-Schäffer, "Optimal control for maximizing link velocity of robotic variable stiffness joints," in *IFAC World Congress*, 2011, pp. 6863–6871.

[6] M. Garabini, A. Passaglia, F. Belo, P. Salaris, and A. Bicchi, "Optimality principles in stiffness control: The vsa kick," in *Robotics and Automation (ICRA), IEEE International Conference on*, 2012, pp. 3341–3346.

[7] M. H. David J. Braun and S. Vijayakumar, "Exploiting variable stiffness in explosive movement tasks," *Robotics: Science and Systems*, 2011.

[8] F. Petit and A. Albu-Schaffer, "State feedback damping control for a multi dof variable stiffness robot arm," in *Robotics and Automation (ICRA), IEEE International Conference on*, 2011, pp. 5561–5567.

[9] A. Ajoudani, N. G. Tsagarakis, and A. Bicchi, "Tele-impedance: Towards transferring human impedance regulation skills to robots," in *International Conference of Robotics and Automation - ICRA*, Saint Paul, MN, USA, May 14 - 18 2012, pp. 382 – 388.

[10] D. Lakatos, F. Petit, and A. Albu-Schaffer, "Nonlinear oscillations for cyclic movements in variable impedance actuated robotic arms," in *Robotics and Automation (ICRA), 2013 IEEE International Conference on*. IEEE, 2013, pp. 508–515.

[11] L. S. Pontryagin, *Mathematical theory of optimal processes*. CRC Press, 1987.

[12] M. Garabini, A. Passaglia, F. Belo, P. Salaris, and A. Bicchi, "Optimality principles in variable stiffness control: The vsa hammer," in *Intelligent Robots and Systems (IROS), 2011 IEEE/RSJ International Conference on*, Sept 2011, pp. 3770–3775.

[13] F. Petit, C. Ott, and A. Albu-Schaffer, "A model free approach to vibration suppression for intrinsically elastic robots," in *Robotics and Automation (ICRA), IEEE International Conference on*, 2014, pp. 2176–2182.

[14] M. G. Catalano, G. Grioli, M. Garabini, F. Bonomo, M. Mancini, N. Tsagarakis, and A. Bicchi, "Vsa - cubebot. a modular variable stiffness platform for multi degrees of freedom systems," 2011.

[15] qb robotics s.r.l. (2013). [Online]. Available: http://www.qbrobotics.com

[16] M. W. Spong, "Underactuated mechanical systems," in *Control Problems in Robotics and Automation*, vol. 230. Springer-Verlag, 1998, pp. 135–150.

[17] M. Scheint, M. Sobotka, and M. Buss, "Compliance in gait synthesis: Effects on energy and gait," in *8th IEEE-RAS International Conference on Humanoid Robots*, 2008, pp. 259–264.

[18] K. Mombaur, R. Longman, H. Bock, and J. Schlöder, *Optimizing Spring-Damper Design in Human-like Walking that is Asymptotically Stable Without Feedback*. Springer, 2008, pp. 403–418.

[19] W. Chen, C. Xiong, M. Liu, and L. Mao, "Characteristics analysis and mechanical implementation of human finger movements," in *Robotics and Automation (ICRA), 2014 IEEE International Conference on*, May 2014, pp. 403–408.

[20] A. V. Rao, D. A. Benson, C. Darby, M. A. Patterson, C. Francolin, I. Sanders, and G. T. Huntington, "Algorithm 902: Gpops, a matlab software for solving multiple-phase optimal control problems using the gauss pseudospectral method," *ACM Transactions on Mathematical Software*, vol. 37, no. 2, Apr. 2010.

[21] A. Velasco, G. M. Gasparri, M. Garabini, L. Malagia, P. Salaris, and A. Bicchi, "Soft-actuators in cyclic motion: Optimization of stiffness and pre-load," in *13th IEEE-RAS International Conference on Humanoid Robots*, October 2013.

[22] M.Fliess and H. Sira-Ram, "State reconstructors: a possible alternative to asymptotic observers and kalman filters," in *Computation Engineering in Systems Applications (CESA)*, 2003.

[23] J. Hoffmann, "Anticipatory behavioral control," in *Anticipatory behavior in adaptive learning systems*. Springer, 2003, pp. 44–65.

[24] R. Shadmehr and F. A. Mussa-Ivaldi, "Adaptive representation of dynamics during learning of a motor task," *The Journal of Neuroscience*, vol. 14, no. 5, pp. 3208–3224, 1994.

[25] D. Bristow, M. Tharayil, A. G. Alleyne *et al.*, "A survey of iterative learning control," *Control Systems, IEEE*, vol. 26, no. 3, pp. 96–114, 2006.

[26] B. Siciliano, L. Sciavicco, L. Villani, and G. Oriolo, *Robotics: modelling, planning and control*. Springer Science & Business Media, 2009.

[27] A. E. Bryson, *Applied optimal control: optimization, estimation and control*. CRC Press, 1975.

[28] J. Shou, D. Pi, and W. Wang, "Sufficient conditions for the convergence of open-closed-loop pid-type iterative learning control for nonlinear time-

varying systems," in *Systems, Man and Cybernetics, 2003. IEEE International Conference on*, vol. 3. IEEE, 2003, pp. 2557–2562.

[29] qbrobotics, "qbmove v0.1 (maker pro) datasheet," datasheet, 2014. [Online]. Available: http://www.naturalmachinemotioninitiative.com

[30] L. Rey and R. Clavel, "The delta parallel robot," in *Parallel Kinematic Machines*. Springer, 1999, pp. 401–417.